Epilepsy-related CDKL5 deficiency slows synaptic vesicle endocytosis in central nerve terminals

Epilepsy-related CDKL5 deficiency slows synaptic vesicle endocytosis in central nerve terminals

Abbreviated Title: CDKL5 is required for synaptic vesicle endocytosis

Christiana Kontaxi[1,2,3], Daniela Ivanova[1,2,3], Elizabeth C. Davenport[1,2,3], Peter C. Kind[1,2,3], Michael A. Cousin[1,2,3*]

[1]Centre for Discovery Brain Sciences, University of Edinburgh, Edinburgh, Scotland, United Kingdom, EH8 9XD

[2]Muir Maxwell Epilepsy Centre, University of Edinburgh, Edinburgh, Scotland, United Kingdom, EH8 9XD

[3]Simons Initiative for the Developing Brain, University of Edinburgh, Edinburgh, Scotland, United Kingdom, EH8 9XD

*Corresponding author

Email: m.cousin@ed.ac.uk

Number of pages: 52

Number of figures: 9

Number of tables: 1

Number of words - Abstract: 149

Number of words - Introduction: 629

Number of words - Discussion: 1268

The authors declare no competing financial interests.

Acknowledgements

This work was supported by grants from the Loulou Foundation, the Simons Foundation (529508), The Wellcome Trust (204954/Z/16/Z) and a College of Medicine and Veterinary Medicine studentship to CK. For the purpose of open access; the author has applied a CC-BY public copyright license to any author accepted manuscript version arising from this submission. We thank Lynsey Dunsmore for help with maintenance of the *Cdkl5* KO LE colony, Dr. Sally Till for her help with the cortices dissection, and Marios Kalomenopoulos for his help with photobleaching correction. We also thank Prof. Ira Milosevic and Prof. Giles Hardingham for useful suggestions in an earlier version of this work.

Abstract

Cyclin-dependent kinase-like 5 (CDKL5) deficiency disorder (CDD) is a severe early-onset epileptic encephalopathy resulting mainly from *de novo* mutations in the X-linked *CDKL5* gene. To determine whether loss of presynaptic CDKL5 function contributes to CDD, we examined synaptic vesicle (SV) recycling in primary hippocampal neurons generated from *Cdkl5* knockout rat males. Using a genetically-encoded reporter, we revealed that CDKL5 is selectively required for efficient SV endocytosis. We showed that CDKL5 kinase activity is both necessary and sufficient for optimal SV endocytosis, since kinase-inactive mutations failed to correct endocytosis in *Cdkl5* knockout neurons, whereas the isolated CDKL5 kinase domain fully restored SV endocytosis kinetics. Finally, we demonstrated that CDKL5-mediated phosphorylation of amphiphysin 1, a putative presynaptic target, is not required for CDKL5-dependent control of SV endocytosis. Overall, our findings reveal a key presynaptic role for CDKL5 kinase activity and enhance our insight into how its dysfunction may culminate in CDD.

Significance statement

Loss of cyclin-dependent kinase like 5 (CDKL5) function is a leading cause of monogenic childhood epileptic encephalopathy. However, information regarding its biological role is scarce. In this study, we reveal a selective presynaptic role for CDKL5 in synaptic vesicle (SV) endocytosis and that its protein kinase activity is both necessary and sufficient for this role. The isolated protein kinase domain is sufficient to correct this loss of function, which may facilitate future gene therapy strategies if presynaptic dysfunction is proven to be central to the disorder. It also reveals that a CDKL5-specific substrate is located at the presynapse, the phosphorylation of which is required for optimal SV endocytosis.

Introduction

The majority of neuronal communication occurs at synapses, at which the presynapse contains an abundant number of synaptic vesicles (SVs) loaded with neurotransmitters that are generally released in response to neuronal activity. Following SV fusion, synchronized mechanisms of SV regeneration from the presynaptic plasma membrane guarantee the availability of readily releasable SVs upon repetitive firing and, hence, the fidelity of neurotransmission (Soykan et al., 2016; Cousin, 2017). Neurodevelopmental disorders affect more than 3 % of children worldwide and involve the disturbance of programmed brain development leading to cognitive, social and motor deficits with epileptic seizures being a frequently observed comorbidity (Thapar et al., 2017; Parenti et al., 2020). Mutations in several genes encoding for SV proteins have been identified as causal in the human condition (Dhindsa et al., 2015; Serajee and Huq, 2015; Baker et al., 2018; Fassio et al., 2018; Salpietro et al., 2019). In addition, multiple animal models that exhibit SV trafficking deficits display abnormalities reminiscent of neurodevelopmental conditions (Di Paolo et al., 2002; Boumil et al., 2010; Koch et al., 2011). Therefore, presynaptic dysfunction is emerging as a high-risk factor during neural development.

Cyclin-dependent kinase-like 5 (CDKL5) deficiency disorder (CDD) is a neurodevelopmental and epileptic encephalopathy that is primarily caused by *de novo* single-nucleotide mutations in the X-linked *CDKL5* gene (Fehr et al., 2013). CDD patients largely experience early-onset epileptic seizures and severe neurodevelopmental delay, in addition to a broad spectrum of other clinical manifestations. The human neuron-specific isoform of CDKL5 is a widely expressed serine/threonine kinase, consisting of an N-terminal catalytic domain followed by a long unstructured C-terminal tail (Kilstrup-Nielsen et al., 2012). CDKL5 has been implicated

in various neuronal activities, including axon elongation (Nawaz et al., 2016), and synaptogenesis (Zhu et al., 2013). Furthermore, it is proposed to have synaptic roles, with hyperexcitability reported in both excitatory and inhibitory *Cdkl5* conditional knockout (KO) neurons (Tang et al., 2017; Tang et al., 2019). Likewise, upon loss of CDKL5, decreased spontaneous glutamate and GABA efflux is observed in cerebellar synaptosomes (Sivilia et al., 2016). However, a direct role for CDKL5 in SV recycling has not been explored.

Almost all pathogenic mutations in the *CDKL5* gene cluster within the region encoding its kinase domain (Hector et al., 2017), suggesting loss of its enzyme function may be key in CDD. Recently, a limited number of endogenous CDKL5 substrates were identified (Baltussen et al., 2018; Munoz et al., 2018), in addition to a series of *in vitro* targets (Sekiguchi et al., 2013; Baltussen et al., 2018). To date, the only *in vitro* presynaptic target of CDKL5 is amphiphysin 1 (Amph1), on the site serine 293 (S293) within a proline-rich domain (PRD). Amph1 is a cytosolic protein highly enriched in nerve terminals, where it acts as a hub during SV recycling via its multiple interaction domains, including its PRD (Wigge and McMahon, 1998; Wu et al., 2009). Importantly, S293 is a major *in vivo* phosphorylation site on Amph1 and is dephosphorylated during neuronal activity, indicating that it may be of high biological importance (Craft et al., 2008).

In the present study, we use a novel *Cdkl5* KO rat model (de Oliveira et al., 2022) to examine SV recycling in CDKL5-deficient hippocampal neurons. Using the genetically-encoded fluorescent reporter synaptophysin-pHluorin (sypHy), we reveal that SV endocytosis is slower upon loss of CDKL5, but SV exocytosis remains unaffected. Following a molecular replacement strategy we demonstrate that the kinase activity of CDKL5 is both necessary and sufficient to correct dysfunction in SV endocytosis. Finally, we determined that the phosphorylation status

of Amph1-S293 remains unaltered in CDKL5-null neurons, revealing that CDKL5 exerts its effect on SV endocytosis via a distinct presynaptic substrate. Taken together, our work reveals that CDKL5-mediated phosphorylation is critical for SV endocytosis efficiency, and that CDKL5 deficiency is responsible for presynaptic malfunction.

Material and methods

Experimental models

All experimental procedures were conducted according to the UK Animal (Scientific Procedures) Act 1986 on the protection of animals used for scientific purposes and were approved by the Animal Welfare and Ethical Review Body at the University of Edinburgh (Home Office project license to M. Cousin – PP5745138 or D. Wyllie - P1351480E). Adult animals were killed by exposure to increasing CO_2 concentration followed by cervical dislocation, while embryos were killed by decapitation followed by destruction of the brain. All animals were maintained on a 12-hour light/dark cycle under constant temperature, with food and water provided when needed.

Cdkl5 KO Long-Evans rats were generated by Horizon Discovery, USA, following a CRISPR interference approach to delete 10 bp in exon 8 of the *Cdkl5* gene (138367-76 in genomic sequence) that results in the introduction of an early stop codon (de Oliveira et al., 2022). *Cdkl5* heterozygous females (*Cdkl5*$^{+/-}$) were crossed with WT Long-Evans males (*Cdkl5*$^{+/y}$) and the offspring were obtained from pregnant females at E17-E19. Prior to genotyping, embryos were sexed by dissecting the abdomen to reveal their inner reproductive organs. Male *Cdkl5*$^{-/y}$ embryos (referred to as CDKL5 KO) and male WT littermate controls were used for neuronal cultures. WT and CDKL5 KO adult (> 2 months old) male rats were used for biochemistry experiments. For CV analysis, primary hippocampal cultures were prepared from WT mouse

embryos (C57BL/6J; Charles River, UK) at E16-18. For the pull-down assay, synaptosomal lysates were generated from Sprague Dawley adult rats (Charles River, UK).

Genotyping

Genomic DNA was obtained from nose or tail biopsies of embryos with alkaline reagent containing 25 mM NaOH and 0.2 mM disodium EDTA (pH 12) at 95 ^{o}C (HotSHOT). DNA extract (1 µl) was used for genotyping with the following primers (Eurogentec, BE): 5'-GGGCTTGTAGCAAATCCATCC-3' (sense), 5'-ATACGTGGCTACTCGGTGGTAC-3' (sense; matching 10 bp deletion), and 5'-AGCAAGCAGAGTTCTATTTTCCT-3' (antisense) using polymerase chain reaction.

DNA constructs

The plasmid DNA vectors in this study were obtained as follows: sypHy from Prof. L. Lagnado (University of Sussex, UK), full-length human CDKL5_1 (hCDKL5_1; referred to as CDKL5) from Dr. V. Kalscheuer (Max Planck Institute for Molecular Genetics, Berlin, DE), full-length rat Amph1 from Dr. H. T. McMahon (MRC Laboratory of Molecular Biology, Cambridge, UK), and pGEX-KG from Dr. C. Rickman (Heriot-Watt University, Edinburgh, UK). Syp1-mCerulean (mCer) was generated as described previously (Gordon et al., 2011).

mCer-C1-CDKL5 was generated by subcloning CDKL5 into an mCer-C1 vector, where the original GFP moiety was replaced by mCer (Gordon and Cousin, 2013), with the primers 5'-CATCATCTCGAGGAATGAAGATTCCTAACATTGGTAATG-3' (sense) and 5'-CATCATGGTACCTTACAAGGCTGTCTCTTTTAAATC-3' (antisense) with restriction sites underlined. Deletion mutants of CDKL5 were generated using the subsequent primers: 5'-CATCATCTCGAGTAATGAAGATTCCTAACATTGG-3' (sense) and 5'-

ATGATGGAATTCCTAAAATGTAGGGTGATTCAAAC-3' (antisense) for the kinase domain (residues 1-297) and 5'-CATCATCTCGAGTACAAACCCAGAGACTTCTGG-3' (sense) and 5'-ATGATGGGTACCTTACAAGGCTGTCTCTTTTAAATC-3' (antisense) for the C-terminal tail (residues 298-960) with restriction sites underlined. Point mutations were introduced into CDKL5 using standard site-directed mutagenesis protocols with the following primers: 5'-GAAATTGTGGCGATCCGGAAATTCAAGGACAGT-3' (sense) and 5'-ACTGTCCTTGAATTTCCGGATCGCCACAATTTC-3' (antisense) for K42R and 5'-GCCACCAGATGGTATCCGTCCCCAGAACTCTTA-3' (sense) and 5'-TAAGAGTTCTGGGGACGGATACCATCTGGTGGC-3' (antisense) for R178P with mutated sites underlined. GST-Amph1 was generated by subcloning Amph1 (residues 248-620) into a pGEX-KG vector using the primers 5'-CATCATGAATTCTAGGAGCTCCCAGTGATTCGGGTC-3' (sense) and 5'-ATGATGCTCGAGCTAAGGAGGCAGTTCCTGAGCGG-3' (antisense) with restriction sites underlined. Point mutations were introduced into Amph1 using standard site-directed mutagenesis protocols with the following primers: 5'-CCAGTGCGACCCAGAGCACCTTCACAGACAAGG-3' (sense) and 5'-CCTTGTCTGTGAAGGTGCTCTGGGTCGCACTGG-3' (antisense) for S293A and 5'-CCAGTGCGACCCAGAGAACCTTCACAGACAAGG-3' (sense) and 5'-CCTTGTCTGTGAAGGTTCTCTGGGTCGCACTGG-3' (antisense) for S293E with mutated sites underlined. All constructs were validated by Sanger sequencing.

Neuronal cultures and transfection

Hippocampi were dissected from CDKL5 KO male embryos and littermate controls and dissociated in papain (10.5 U/ml; Worthington Biochemical Corporation; #LK003178). Tissue was triturated in Dulbecco's Modified Eagle Medium/Nutrient Mixture F-12 (Gibco; #21331-

020) supplemented with 10 % (v/v) foetal bovine serum (BioSera; #S1810-500). Following a low-speed centrifugation, neurons were resuspended in Neurobasal medium (Gibco; #21103-049) supplemented with 0.5 mM L-glutamine (Gibco; #25030-024), 1 % (v/v) B-27 supplement (50X, serum free; Gibco; #17504044), and penicillin/streptomycin (Gibco; #15140-122). Neurons were plated on poly-D-lysine (Sigma-Aldrich; #P7886)- and laminin (Sigma-Aldrich; #L2020)-precoated coverslips and kept in supplemented Neurobasal medium in a humidified incubator at 37 °C/5 % CO_2 for up to 15 days. The mitotic inhibitor cytosine β-D-arabinofuranoside (Sigma-Aldrich; #C1768) was added to neurons at 1 µM on 3 days *in vitro* (DIV) to prevent glial proliferation. This ensures that sufficient astrocytes are present to support neuronal development. Neurons were transfected after 8-9 DIV with Lipofectamine 2000 (Thermo Fisher Scientific; #11668027) as per manufacturer's instructions.

Live-cell imaging and data analysis

Primary hippocampal neurons at 13-15 DIV were mounted in a closed bath imaging chamber (Warner; #RC-21BRFS) allowing electrical field stimulation (1ms pulse width, 100 mA current output). Tyrode's buffer (119 mM NaCl, 2.5 mM KCl, 2 mM $CaCl_2$, 2 mM $MgCl_2$, 25 mM HEPES, 30 mM glucose, pH 7.4), supplemented with 10 µM 6-cyano-7-nitroquinoxaline-2,3-dione (CNQX; Abcam; ab120271) and 50 µM DL-2-amino-5-phosphonopentanoic acid (AP5; Abcam; ab120044), was perfused continuously. At the end of each recording, neurons were perfused with 50 mM NH_4Cl solution, pH 7.4, substituting equal concentration of NaCl in Tyrode's buffer. All recordings were performed at room temperature. Transfected neurons were visualized using a Zeiss Axio Observer D1 inverted epifluorescence microscope (Zeiss Ltd., Germany) with a 40x 1.3 NA oil immersion objective. Time-lapse images were acquired using a Hamamatsu Orca-ER camera and the acquisition rate was set at 4 s constantly pre- and post-

stimulation. Neurons expressing sypHy and mCer constructs were imaged at 500 nm and 430 nm excitation, respectively, using a 525-nm dichroic and a 535-nm emission filter. To measure exocytosis rate, Tyrode's buffer was supplement with 1 µM bafilomycin A1 (Alfa Aesar; #J61835.MX). To measure acidification kinetics, HEPES was replaced by 25 mM 2-(N-morpholino)ethanesulfonic acid in Tyrode's buffer and acquisition rate was set at 2 s. A Zeiss Axio Observer Z1 inverted epifluorescence microscope with a 40x 1.3 NA oil immersion objective (Zeiss Ltd., Germany), a Colibri 7 LED light source (Zeiss Ltd., Germany), and an AxioCam 506 camera (Zeiss Ltd., Germany) were used for the experiment where neurons were challenged with 20 action potentials (APs). Neurons expressing sypHy were imaged at 450-490 nm excitation (495-nm dichroic, 500-550-nm emission) with the acquisition rate set at 500 ms.

Time-lapse stacks of images were analysed using the Fiji is just ImageJ (Fiji) software (Schindelin et al., 2012; Schneider et al., 2012). These were initially aligned using the StackReg plugin with Rigid Body transformation type (Thevenaz et al., 1998). Regions of interest of 0.8 µm in diameter were placed on presynaptic boutons responsive to stimulation. Fluorescence intensity was measured for all image slices using the Times Series Analyzer (https://bit.ly/3M5hWpb). The average $\Delta F/F_0$ was calculated for each coverslip and was normalised to the maximum fluorescence intensity either during stimulation or NH_4Cl perfusion. A one-phase exponential fit was used to correct baseline for bleaching that was subtracted from all time points. Distance to the baseline at fixed time after termination of stimulation was used as a measure of endocytosis speed. No background was subtracted. For the 20 APs experiment, due to extensive photobleaching, we applied a correction that consists of a rotation of the average curves anti-clockwise with respect to the normalised

stimulation peak. This correction preserved the biological information and was done only for presentation purposes.

Immunocytochemistry

Primary cultured hippocampal neurons were fixed with 4 % (w/v) paraformaldehyde/PBS for 10 min and neutralized with 50 mM NH_4Cl/PBS for 10 min. After washing with PBS, neurons were permeabilized in 0.1 % (v/v) Triton X-100, 1 % (w/v) bovine serum albumin (Roche Diagnostics GmbH; #10735078001)/PBS for 5 min and blocked in 1 % (w/v) bovine serum albumin/PBS for 30 min. Following blocking, neurons were incubated with the appropriate dilution of primary antibodies for 1-2 h at room temperature. Primary antibodies were used as follows: sheep anti-CDKL5 (human epitope; 1:200; Rouse lab, University of Dundee, UK), chicken anti-GFP (1:5000; Abcam; #ab13970), rabbit SV2A (1:200; Abcam; #ab32942), and guinea pig anti-VGLUT1 (1:1000; Synaptic Systems; #135 304). Alexa Fluor secondary antibodies (1:1000; Molecular Probes, Thermo Fisher Scientific) were applied for 1-2 h at room temperature in the dark, including donkey anti-rabbit Alexa Fluor 488 (#A-21206), donkey anti-sheep Alexa Fluor 568 (#A-21099), goat anti-chicken Alexa Fluor 488 (#A-11039), and goat anti-guinea pig Alexa Fluor 568 (#A-11075).

Transfected neurons were visualized using a Zeiss Axio Observer Z1 inverted epifluorescence microscope (Zeiss Ltd., Germany) and a 40x 1.3 NA oil immersion objective at 480 nm and 550 nm excitation wavelengths. Fluorescent light was detected at 500-552 nm and >565 nm using a 495-nm and a 565-nm dichroic filter, respectively. Neurons expressing mCer-tagged constructs were visualized at 480 nm excitation wavelength using the anti-GFP antibody described above. Images were acquired using a Zeiss AxioCam 506 camera and Zeiss ZEN 2 software. Data analysis was performed using Fiji. To quantify endogenous CDKL5 expression,

regions of interest were drawn manually around mCer-expressing cell bodies and average CDKL5 signal was calculated and normalised to that of untransfected cell bodies. Background was subtracted in all cases. For counting bouton numbers, MaxEntropy thresholding was applied and positive accumulations of 0.64-2.24 µm in diameter were counted using the Analyze particles plugin (Kapur et al., 1985). The number of SV2A- and VGLUT1-positive puncta was counted in (50 x 15) μm^2 selections along neuronal processes to eliminate the influence of neuronal density variation between genotypes. For CV analysis, the mean GFP fluorescence along an axonal segment of > 15 µm was divided by the standard deviation and expressed as a percentage (Gordon and Cousin, 2013). The average CV value of five axonal segments was calculated per field of view.

Biochemical isolation of crude SVs

The crude purification of SVs was performed as described previously (Huttner et al., 1983). An adult rat brain was homogenized in ice-cold 0.32 M sucrose, 5 mM EDTA (pH 7.4) after removing the cerebellum. The homogenate (H) was centrifuged twice at 950 x *g* for 10 min at 4 °C and the supernatant was collected each time. The combined supernatant (S1) was spun at 20,400 x *g* for 30 min at 4 °C. The pellet (P2) represents the crude synaptosomal fraction. For crude isolation of SVs, the P2 fraction was resuspended in ice-cold 0.32 M sucrose/EDTA and incubated with 1 M HEPES/NaOH solution (pH 7.4) on ice for 30 min. After spinning at 32,900 x *g* for 20 min at 4 °C, the lysate pellet (LP1) and lysate supernatant (LS1) were obtained. The supernatant was then centrifuged at 268,000 x *g* for 2 h at 4 °C to generate LS2 and LP2 fractions. The LP2 pellet that represents the crude SV fraction was collected and resuspended in 40 mM sucrose. Aliquots of the intermediate fractions were kept for analysis.

The total protein amount of the samples was measured by Bradford (AppliChem; #A6932) and their concentration was adjusted to 1 mg/ml prior to Western blot analysis.

Immunoprecipitation

Adult rat brain was mechanically homogenized in buffer containing 50 mM HEPES (pH 7.5), 0.5 % (v/v) Triton X-100, 150 mM NaCl, 1 mM EDTA, 1 mM EGTA, 1 mM phenylmethylsulfonyl fluoride, and protease inhibitor cocktail (Sigma-Aldrich; #P8849). The homogenate was incubated for 1-2 h at 4 ^{o}C rotating and then centrifuged at 155,000 x *g* for 40 min at 4 ^{o}C. The supernatant was collected and pre-cleaned with Protein G Agarose beads (Sigma-Aldrich; #11719416001) for 1-2 h at 4 ^{o}C rotating to enhance specificity and the total protein content was quantified by Bradford assay. The brain lysate (equivalent to 2 mg of protein) was incubated with 2-4 µg of the antibody of interest at 4 ^{o}C rotating overnight. Next, Protein G Agarose beads (approximately 20 µl) were added to the antibody-containing brain lysates and left rotating for 1-2 h at 4 ^{o}C prior to being centrifuged at low speed. The supernatant was then discarded and after three washes in HEPES buffer, Laemmli sample buffer was added directly to the beads followed by heating at 95 ^{o}C for 5 min. A random antibody against Eps15 Homology Domain protein (EHD; goat anti-EHD; Santa Cruz Biotechnology; #sc-23452) was used as a control.

Drug treatments

Cyclosporin A (Sigma-Aldrich; #30024), calyculin A (Abcam; ab141784), PD98059 (EMD Millipore Corp.; #513000-5MG) and roscovitine (EMD Millipore Corp.; #557360-1MG) were dissolved in dimethyl sulfoxide (DMSO; Sigma-Aldrich; #D8418), whereas AP5, CNQX, and EGCG (Calbiochem, #324880-10MG) in ultrapure water for stock concentration. For all drug experiments, culture medium was replaced by unsupplemented Neurobasal medium and

neurons were treated with appropriate drug dilution at 37 °C. The drugs were administered as follows: 10 µM cyclosporin A or 100 nM calyculin A for phosphatase inhibition experiments, 50 µM AP5 and 10 µM CNQX for electrical stimulation, 20 mM EGCG, 100 µM PD98059, and 50 µM roscovitine for kinase inhibition experiments. Stimulation was performed at room temperature in the presence of drugs in Tyrode's buffer prior to lysis with Laemmli buffer.

Pull-down assay

Glutathione S-transferase (GST)-fused proteins were expressed in *Escherichia coli* BL21(DE3) cells in lysogeny broth medium containing ampicillin after induction with 1 mM isopropyl β-D-1-thiogalactopyranoside (Calbiochem; #420322). Induced bacterial cultures were spun at 5000 x *g* for 15 min at 4 °C and the pellets were resuspended in ice-cold buffer containing 10 mM Tris, 150 mM NaCl, 1 mM EDTA, pH 8, protease inhibitors and 1 mM phenylmethylsulfonyl fluoride. Lysozyme (0.0675 µg/µl; Sigma-Aldrich; #L6876), 4 mM dithiothreitol (Sigma-Aldrich; #D0632), and 10 % (v/v) Triton X-100 were also added. The cells were sonicated at 10 kHz and the clear lysates were spun at 17,420 x *g* for 10 min at 4 °C. The supernatant was transferred to pre-washed Glutathione Sepharose 4B beads (GE Healthcare; #GE17-0756-01) resuspended in PBS to create a 50 % suspension and left rotating overnight at 4 °C. A small volume of glutathione -coupled GST-fused proteins was loaded into a ProbeQuant G-50 Micro Column (GE Healthcare; #28903408) and washed once in ice cold lysis buffer containing 1 % (v/v) Triton X-100, 25 mM Tris-HCl, 150 mM NaCl, 1 mM EGTA, 1 mM EDTA, pH 7.4, prior to incubation with synaptosomal lysates. The columns were washed successively in ice cold lysis buffer, in NaCl-supplemented lysis buffer (500 mM) and in 20 mM Tris, pH 7.4. Laemmli sample buffer was added into the columns and the eluted proteins were denatured at 95 °C for 5 min. All GST-coupled Amph1 constructs were devoid of the N-

terminal Bin/Amphiphysin/Rvs (N-BAR) and the Src-homology 3 (SH3) domains and their total level was estimated with Coomassie Brilliant blue (Instant Blue Protein Stain; C.B.S. Scientific; #HG73010) staining prior to Western blot analysis.

Western blotting

Brain samples were prepared as described above, whereas hippocampal neurons at 14-15 DIV were lysed directly with Laemmli sample buffer. Proteins were denatured at 95 ^{o}C for 5 min. Protein extracts were separated by SDS-PAGE, transferred to a nitrocellulose membrane, and blocked in Intercept (PBS or TBS) blocking buffer (LI-COR Biosciences; #927-70001 or 927-60001). Membranes were incubated with primary antibodies at 4 ^{o}C overnight and IRDye secondary antibodies (1:10000) for 2 h at room temperature in Intercept (PBS or TBS) blocking buffer containing 0.1 % (v/v) Tween-20 in the dark. Blots were visualized using the LI-COR Biosciences Odyssey Infrared Imaging System and quantification of band densities was performed using the Image Studio Lite version 5.2 software (LI-COR Biosciences; SCR_013715) with background subtraction or Fiji. Equal protein amount loading was verified by Ponceau-S (Sigma-Aldrich; #P7170) staining. The primary (phospho)antibodies that were used in this study are: sheep CDKL5 (human epitope; 1:500; Rouse lab, University of Dundee, UK), sheep CDKL5 (mouse epitope; 1:500; Rouse lab, University of Dundee, UK), rabbit anti-CDKL5 (1:500; Atlas Antibodies; #HPA002847), goat anti-Amph1 (1:500; Santa Cruz Biotechnology; #sc-8536), goat anti-CHC (1:250; Santa Cruz Biotechnology; #sc-6579), goat anti-syndapin 1 (1:1000; Santa Cruz Biotechnology; #sc-10412), guinea pig anti-VGLUT1 (1:2000; Synaptic Systems, #135 304), rabbit anti-ATP6V1B2 (1:5000; Abcam; ab183887), goat anti-Dyn1 (1:500; Santa Cruz Biotechnology; #sc-6402), goat endophilin A1 (1:1000; Santa Cruz Biotechnology; sc-10874), rabbit Syp1 (1:500; Abcam; ab14692), mouse PSD95 (1:1000; BioLegend;

#810401), mouse β-actin-peroxidase (1:30000; Sigma-Aldrich; #A3854), rabbit pMAP1S-S900 (light chain) (1:50; Rouse lab, University of Dundee, UK), sheep pDyn1-S774 (1:1000; AbD Serotec, Bio-rad, #AHP899), rabbit pAkt-S473 (1:1000; Cell signalling; #9018), rabbit pGSK3α/β-S9/S21 (1:1000; Cell signalling; #9331). For experiments assessing the phosphorylation levels of Amph1-S293, a rabbit polyclonal phosphoantibody was raised against the peptide PVRPRS^{293}PSQTRC of Amph1 (0.5 mg/ml; MRC Protein Phosphorylation Unit, University of Dundee, UK). Secondary antibodies (1:10000) were used for 2 h at room temperature in the dark, including donkey anti-goat IRDye 680RD (#925-68074), donkey anti-goat IRDye 800CW (#925-32214), donkey anti-guinea pig IRDye 680RD (#925-68077), donkey anti-mouse IRDye 680RD (#925-68072), donkey anti-mouse IRDye 800CW (#925-32212), donkey anti-rabbit IRDye 680RD (#925-68073), donkey anti-rabbit IRDye 800CW (#925-32213) from LI-COR Biosciences, and rabbit anti-sheep IRDye800 conjugated (Rockland Immunochemicals; #613732168).

Experimental design and statistical analysis

Statistical calculations were conducted using GraphPad Prism 8.4.2 (GraphPad Software Inc; SCR_002798). The normality of the data distribution was assessed by performing D'Agostino and Pearson omnibus normality test with significance level set at $\alpha = 0.05$. Datasets following a Gaussian distribution were presented as mean ± standard error of the mean (SEM) and statistical significance was assessed by two-tailed unpaired *t* test for comparison between two groups or analysis of variance (ANOVA) followed by Tukey's, Dunnett's or Sidak's post hoc analysis for multiple comparisons. Datasets following a non-Gaussian distribution were presented as median with interquartile range (IQR) indicating min to max whiskers and statistical significance was evaluated by Mann-Whitney test for comparison between two

groups or Kruskal-Wallis followed by Dunn's post hoc analysis for multiple comparisons. For experiments with a small number of replicates for a normality test to be performed, a parametric test was assumed. Asterisks refer to *p*-values as follows: *; $p \leq 0.05$, **; $p \leq 0.005$, ***; $p \leq 0.001$, ****; $p \leq 0.0001$. All experiments consisted of at least three independent biological replicates. Live-imaging data were analysed blind for experiments consisting of two groups. Random variation or effect size were not estimated. Sample size and statistical test are indicated in the figure legends. Detailed description of the statistical tests and *p* values are presented in Table 1.

Results

Endogenous CDKL5 is sorted into the presynaptic terminal

CDKL5 is a ubiquitous neuronal protein kinase (Rusconi et al., 2011; Schroeder et al., 2019) however, its localisation at the nerve terminal has not been extensively addressed. To verify that CDKL5 is present in presynaptic terminals, and therefore in the correct location to influence SV recycling, a classical subcellular fractionation was performed. During this protocol, an adult rat brain was subjected to homogenisation and differential centrifugation to generate distinct subcellular fractions, including a crude synaptosome- (P2, mainly representing the presynapse with attached postsynaptic density) and an SV-enriched (LP2) fraction. Western blotting with a CDKL5-specific antibody (Figure 1A) revealed that CDKL5 was present in the P2 fraction and enriched in the LP2 fraction, where the SV protein synaptophysin 1 (Syp1) also accumulated (Figure 1B). The relative absence of the postsynaptic marker, postsynaptic density 95 (PSD95), suggested that contamination of the LP2 fraction with postsynaptic elements was limited. Therefore, CDKL5 is present at presynaptic terminals and may associate with SVs, consistent with previous studies showing that CDKL5 co-localises with the presynaptic vesicular glutamate transporter 1 (VGLUT1) in mouse neurons (Ricciardi et al., 2012; Wang et al., 2021).

To assess whether CDKL5 is targeted exclusively to nerve terminals or displays a more diffuse axonal distribution, we performed coefficient of variation (CV) analysis. Hippocampal neurons were transfected with either CDKL5 fused to the fluorescent protein mCer (mCer-CDKL5), Syp1-mCer or the empty mCer vector and were then immunolabelled for the presence of the

fluorescent tag (Figure 1C). SV proteins, such as Syp1, are anticipated to have a punctate distribution along the axon and therefore a higher CV value. In contrast, lower CV values indicate a homogeneous distribution of a protein along the axon. In agreement, mCer-Syp1 displayed a localised distribution along the axon and a high CV value, in agreement with previous results (Gordon and Cousin, 2013). Quantification of the distribution profile of CDKL5 in axonal segments indicated a CV value similar to the empty mCer vector (Figure 1D, one-way ANOVA followed by Tukey's multiple comparison test - mCer vs Syp1-mCer $p < 0.0001$, mCer vs mCer-CDKL5 $p = 0.0640$. Syp1-mCer vs mCer-CDKL5 $p < 0.0001$). Therefore, CDKL5 is diffusely distributed along the axon, including presynaptic terminals.

Loss of CDKL5 does not influence the levels of presynaptic proteins or the number of presynaptic boutons

We next investigated whether the absence of CDKL5 causes any defects in presynaptic stability since disruption of synapse stability/synaptogenesis may result in altered neuronal development. This was important to address, since dysregulation of protein levels in addition to altered synapse number have been reported in mice lacking CDKL5 (Della Sala et al., 2016; Ren et al., 2019; Schroeder et al., 2019; Tang et al., 2019). First, we examined whether expression of key presynaptic proteins was altered in rat CDKL5 KO neurons via Western blotting. Initially, we confirmed the absence of CDKL5 in lysates of KO neurons (Figure 2A, Unpaired two-tailed *t* test – CDKL5 $p < 0.0001$). We then analysed a range of presynaptic molecules including proteins important for SV recycling, such as clathrin heavy chain (CHC), dynamin 1 (Dyn1), endophilin A1, and syndapin 1; integral SV proteins, such as Syp1, VGLUT1, and the v-type proton ATPase subunit B (ATP6V1B2); and phosphoproteins that have been

implicated in the regulation of SV endocytosis, such as the protein kinases glycogen synthase kinase 3 (GSK3) and Akt (Clayton et al., 2010; Smillie and Cousin, 2012; Ferreira et al., 2021). These latter enzymes were of particular interest, since the PI3K/GSK3/Akt pathway has been one of the most perturbed signalling cascades in CDKL5 deficiency model systems (Wang et al., 2012; Amendola et al., 2014; Jiang et al., 2019). This analysis revealed that the absence of CDKL5 did not significantly alter the total protein level of any candidate, or the phosphorylation status (and thus activity) of either GSK3 or Akt when compared to wild-type (WT) controls (Figure 2A, Unpaired two-tailed *t* test – CHC $p = 0.4921$, Dyn1 $p = 0.1808$, Syndapin 1 $p = 0.6711$, Endophilin A1 $p = 0.4505$, VGLUT1 $p = 0.9899$, ATP6V1B2 $p = 0.2114$, Syp1 $p = 0.0592$, pAkt-S473 $p = 0.6186$, pGSK3α/β-S9/21 $p = 0.2271$). Therefore CDKL5 KO neurons do not display overt alterations in presynaptic proteins or signalling cascades.

Next, we investigated whether the lack of CDKL5 led to a reduced number of presynaptic terminals. To achieve this, WT and CDKL5 KO neurons were double-stained for two distinct presynaptic markers, synaptic vesicle protein 2A (SV2A) and VGLUT1, to assess the number of presynaptic boutons and excitatory presynaptic subtypes, respectively. There were no genotype-specific differences in SV2A- and VGLUT1-positive puncta along neuronal processes (Figure 2B). Therefore, there is no effect of the absence of CDKL5 on either the number of total or excitatory presynaptic terminals (Figure 2C, D, Mann Whitney two-tailed *t* test – C, SV2A $p = 0.2854$, D, VGLUT1 $p = 0.2302$). Overall, this data reveals that the formation and maintenance of nerve terminals in rat primary neuronal cultures is not affected upon CDKL5 deficiency.

Loss of CDKL5 impairs SV regeneration but does not influence SV exocytosis

The presynaptic localisation of CDKL5 suggests that CDKL5 is implicated in SV recycling. Indeed, phenotypes reported in mice lacking CDKL5, such as altered spontaneous excitatory / inhibitory synaptic activity (Tang et al., 2017; Wang et al., 2021), and aberrant paired-pulse facilitation (Tang et al., 2019), indicate that CDKL5 deficiency results in defects in synaptic transmission that could be due to dysfunctional SV recycling. To determine this, we used the genetically-encoded reporter sypHy, in which a pH-sensitive form of GFP, ecliptic pHluorin (pKa ~7.1), is inserted into an intravesicular loop of Syp1 (Miesenbock et al., 1998; Granseth et al., 2006). The fluorescence of sypHy is dictated by the pH of its immediate environment, with fluorescence being quenched in the acidic SV lumen, unquenched upon stimulus-dependent SV exocytosis and exposure to the cell surface, and re-quenched following endocytosis and SV acidification (Figure 3A). To determine the potential contribution of CDKL5 to SV recycling across a range of stimulus intensities, primary hippocampal neurons derived from CDKL5 KO rats or WT littermate controls were transfected with sypHy and stimulated with AP trains of either 5 Hz or 10 Hz (both 300 APs), 40 Hz (400 APs), or 10 Hz (20 APs) (Figure 3B, E, H, K). To quantify for the extent of activity-dependent SV exocytosis, the amount of sypHy fluorescence during stimulation was measured as a proportion of the total fluorescence within the presynapse revealed by perfusion with NH_4Cl that allows for an estimation of the total recycling SV pool. We found that the extent of SV exocytosis remained unaltered between genotypes across all stimulation frequencies investigated (Figure 3C, F, I, L Unpaired two-tailed *t* test - C, $p = 0.8932$, F, $p = 0.3025$, I, $p = 0.6015$, L, $p = 0.3680$).

To confirm this phenotype, we next measured the rate of sypHy fluorescence increase during prolonged stimulation (10 Hz for 90 s) in the presence of bafilomycin A1. Bafilomycin A1 is a V-type ATPase inhibitor, and therefore removes any potential contribution from SV endocytosis to the sypHy response during the stimulation by blocking SV acidification (Sankaranarayanan and Ryan, 2001). When this experiment was performed, no difference was observed in either the rate of the sypHy fluorescence increase (SV exocytosis rate) or the extent of the sypHy response (SV recycling pool size) between WT and CDKL5 KO neurons (Figure 4A, B, C, Unpaired two-tailed *t* test – B, $p = 0.3494$, C, $p = 0.3477$). Therefore, SV exocytosis is not altered upon CDKL5 loss.

We next focused on SV endocytosis, in which protein kinases perform an important role (Tan et al., 2003; Clayton et al., 2010). As acidification is a rapid process when compared to rate-limiting SV endocytosis (Atluri and Ryan, 2006; Granseth et al., 2006; Egashira et al., 2015), monitoring the sypHy fluorescence decay after stimulation can be used to estimate SV endocytosis kinetics (Sankaranarayanan and Ryan, 2000). To quantify the kinetics of SV retrieval, the sypHy stimulation peak was normalised, and the amount of sypHy remaining to be retrieved 2 minutes after termination of stimulation was measured. This parameter was used for consistency across protocols, since in specific cases the decay kinetics were not mono-exponential (rendering time constant measurements redundant). CDKL5 KO neurons consistently displayed slower SV endocytosis across all frequencies examined when compared to WT, suggesting that CDKL5 is important for optimal SV endocytosis (Figure 3D, G, J, M Unpaired two-tailed *t* test - D, $p = 0.0022$, G, $p = 0.0065$, J, $p = 0.0442$, M, $p = 0.0409$).

Interestingly, the requirement for CDKL5 appeared to be more prominent at lower stimulation frequencies.

To confirm that this phenotype was due to slowed SV endocytosis and not dysfunctional SV acidification, we determined the kinetics of SV acidification using an acid-pulse protocol (Granseth et al., 2006). In this protocol, an impermeant acid buffer (pH 5.5) is perfused immediately after stimulation to quench all surface sypHy, which exclusively reveals the sypHy signal inside recently retrieved SVs (where the quenching rate can be calculated). In this protocol, WT and CDKL5 KO neurons expressing sypHy are perfused with acid buffer both prior to stimulation (to reveal an initial baseline) and immediately after stimulation (10 Hz, 30 s, to reveal the quenching rate inside SVs) (Figure 4D). No significant difference in the SV acidification rate in neurons lacking CDKL5 compared to WT neurons was apparent (Figure 4E, Unpaired two-tailed *t* test – $p = 0.5061$), confirming that the slowing in the post-stimulus sypHy fluorescence decay in CDKL5 KO neurons was due to impaired SV endocytosis.

CDD is a disorder of early life, and a therefore key question to address is whether defects can be rescued by the re-introduction of the gene, or whether the altered circuit activity in its absence renders gene correction redundant. To address this in our system, we determined whether expression of WT CDKL5 in KO neurons could correct SV endocytosis deficits. Both CDKL5 KO and WT littermate controls were co-transfected with sypHy and either mCer-CDKL5 or an empty mCer vector and stimulated with either 300 APs at 10 Hz or 400 APs at 40 Hz. Analysis of the post-stimulus sypHy response showed that expression of mCer-CDKL5 fully restored the kinetics of SV endocytosis after 10 Hz stimulation and partially after 40 Hz (Figure

5A-D, Two-way ANOVA followed by Tukey's multiple comparison test – B, WT vs KO p = 0.0419, WT vs KO+CDKL5 p = 0.9956, KO vs WT+CDKL5 p = 0.0134, KO vs KO+CDKL5 p = 0.0229, WT+CDKL5 vs KO+CDKL5 p = 0.9947; D, WT vs KO p = 0.0158, WT vs KO+CDKL5 p = 0.5756, KO vs WT+CDKL5 p = 0.0317, KO vs KO+CDKL5 p = 0.3186, WT+CDKL5 vs KO+CDKL5 p = 0.7013). Importantly, mCer-CDKL5 overexpression had no impact on SV endocytosis kinetics in WT neurons, indicating that increased levels of the protein kinase had no dominant negative effect (Figure 5A-D, Two-way ANOVA followed by Tukey's multiple comparison test – B, WT vs WT+CDKL5 p = 0.9644, D , WT vs WT+CDKL5 p = 0.9982). Thus, expression of CDKL5 can restore presynaptic defects observed in KO neurons.

CDD-related mutants of CDKL5 fail to rescue SV endocytosis impairment

As stated above, in CDD all identified missense mutations that are pathogenic are found within the catalytic domain suggesting the disorder is due to loss of its enzymatic function (Hector et al., 2017; Munoz et al., 2018). To determine whether the protein kinase activity of CDKL5 is essential for its role in SV endocytosis, we investigated the ability of two mutant forms of full-length CDKL5 to restore function in CDKL5 KO neurons. The CDKL5 mutants were 1) K42R (a catalytically-inactive form of the enzyme that cannot bind ATP (Lin et al., 2005)), and 2) R178P, a mutation reported in CDD patients of both sexes with severe neurological features (Elia et al., 2008; Nemos et al., 2009) (Figure 6A). CDKL5 KO neurons were co-transfected with sypHy and either WT CDKL5 or one of the CDKL5 mutants and SV endocytosis kinetics were monitored following stimulation with either 300 APs at 10 Hz or 400 APs at 40

Hz (Figure 6B, D). WT CDKL5 fully restored SV endocytosis kinetics after both stimulation trains, as observed previously. In contrast, neither of the CDKL5 mutants were able to correct the SV endocytosis defect (Figure 6C, E, One-way ANOVA followed by Dunnett's multiple comparison test – C, KO vs CDKL5 $p = 0.0006$, KO vs K42R $p = 0.5993$, KO vs R178P $p = 0.6845$, E, KO vs CDKL5 $p = 0.0135$, KO vs K42R $p = 0.9827$, KO vs R178P $p = 0.8653$). The absence of rescue was not due to their low expression, since this was equivalent to the exogenously-expressed WT enzyme (all median (min – max); WT 6.96 (1.81 – 46.13); K42R 8.25 (1.75 – 32.12); R178P 7.15 (1.49 – 33.12); WT vs K42R $p > 0.999$; WT vs R178P $p > 0.999$; Kruskal-Wallis test with Dunn's multiple comparison test). These data reveal that the protein kinase activity of CDKL5 is essential for optimal SV endocytosis kinetics and also associates CDKL5 pathology with defective SV recycling.

The kinase activity of CDKL5 is necessary and sufficient for optimal SV endocytosis

We have revealed an essential requirement for the enzymatic activity of CDKL5 in SV endocytosis. However a key question to address is whether this activity is both necessary and sufficient to correct SV endocytosis dysfunction in CDKL5 KO neurons. To address this, we examined whether expression of the isolated protein kinase domain was sufficient to correct presynaptic function in CDKL5 KO neurons. To determine this, we generated mCer-tagged deletion mutants of CDKL5 comprising either the kinase domain (ΔC; aa 1-297) or the C-terminal tail (Δkinase; aa 298-960) (Figure 7A). Primary cultures of hippocampal CDKL5 KO neurons were co-transfected with sypHy and either full-length CDKL5 or one of the deletion

mutants. Double immunostaining of primary cultured hippocampal neurons for GFP and endogenous CDKL5 suggested that Δkinase was expressed to higher levels than WT, whereas ΔC could not be quantified due to the absence of an antibody epitope (Figure 7B, C, Kruskal-Wallis test followed by Dunn's multiple comparison test – C, mCer vs CDKL5 $p < 0.0001$, mCer vs Δkinase $p < 0.0001$, CDKL5 vs Δkinase $p = 0.0038$). SV endocytosis kinetics were assessed by monitoring sypHy fluorescence after stimulation with 300 APs at 10 Hz or 400 APs at 40 Hz (Figure 7D, F). We observed that the isolated kinase domain was sufficient to rescue SV endocytosis kinetics similarly to full-length CDKL5 at both stimulus intensities (Figure 7E, G, One-way ANOVA followed by Dunnett's multiple comparison test – C, KO vs CDKL5 $p = 0.0044$, KO vs ΔC $p = 0.0010$, E, KO vs CDKL5 $p = 0.0331$, KO vs ΔC $p = 0.0281$). In contrast, the isolated C-terminus could not (Figure 7E, G, One-way ANOVA followed by Dunnett's multiple comparison test – C, KO vs Δkinase $p = 0.4857$, E, KO vs Δkinase $p = 0.9334$), suggesting that this region cannot support SV endocytosis in the absence of the protein kinase domain. Therefore, the ability of the isolated CDKL5 protein kinase domain to correct presynaptic function reveals that it is both necessary and sufficient to rescue SV endocytosis, and that the C-terminal tail is dispensable for this role.

CDKL5-mediated phosphorylation at Amph1-S293 is not required for SV regeneration

Since the kinase activity of CDKL5 is necessary for optimal SV endocytosis, this suggests that there is at least one CDKL5 substrate at the presynapse that mediates this role. The only candidate presynaptic target of CDKL5 that has been identified so far is Amph1, from *in vitro*

studies (Sekiguchi et al., 2013; Katayama et al., 2015). To determine whether Amph1 may be a *bona fide* CDKL5 substrate, we first examined the ability of these two proteins to interact with each other, as it would be anticipated for an enzyme to interact with its substrates, even transiently. We demonstrated reciprocal co-immunoprecipitation of Amph1 and CDKL5 from rat brain lysates (Figure 9A). This indicates that CDKL5 binds to Amph1 *in vivo*, and hence supports that Amph1 may be a CDKL5 substrate.

Previous studies determined Amph1-S293 as the residue phosphorylated by CDKL5 *in vitro* (Sekiguchi et al., 2013; Katayama et al., 2015), which also resides within a CDKL5 consensus motif (Baltussen et al., 2018; Munoz et al., 2018). Furthermore, Amph1-S293 appears to be a plausible CDKL5 target in relation to its potential role in SV endocytosis, since its phosphorylation status regulates the affinity of Amph1 for the presynaptic endocytosis protein endophilin A1 (Murakami et al., 2006; Sekiguchi et al., 2013). To explore CDKL5-mediated phosphorylation of Amph1, we generated a rabbit polyclonal phospho-specific antibody against Amph1-S293 (Figure 8A). To validate this antibody, we generated recombinant GST-conjugated constructs of the central region of WT Amph1 that encompassed this site (residues 248-620, GST-Amph1) and two phospho-mutants, a null (GST-S293A) and a mimetic (GST-S293E) and assessed its specificity by Western blotting. This approach revealed that the pAmph1-S293 antibody reacted exclusively with the phospho-mimetic GST-S293E (Figure 8B), suggesting that the phospho-antibody is highly specific for phosphorylated Amph1-S293.

Amph1 undergoes dephosphorylation coupled to neuronal activity (Bauerfeind et al., 1997; Micheva et al., 1997). Accordingly, Amph1-S293 is one of the phospho-sites that is

551 dephosphorylated following high frequency stimulation (Murakami et al., 2006; Craft et al.,
552 2008). Therefore, we next focused on verifying whether Amph1-S293 was dephosphorylated
553 in an activity-dependent manner. Initially, we treated hippocampal neuronal cultures with 50
554 mM KCl for 2 min to induce neuronal depolarisation. This greatly reduced the signal from the
555 pAmph1-S293 antibody when compared to basal cultures, suggesting that the antibody
556 accurately reports the phosphorylation status of this residue. We next examined whether
557 Amph1-S293 dephosphorylation occurs via calcineurin, since this Ca^{2+}-dependent enzyme
558 dephosphorylates a series of presynaptic proteins during neuronal activity (Nichols et al.,
559 1994; Bauerfeind et al., 1997; Marks and McMahon, 1998; Cousin and Robinson, 2001).
560 Treatment with cyclosporin A, a calcineurin inhibitor, prevented the activity-dependent
561 dephosphorylation at Amph1-S293, confirming that calcineurin performs this role. In
562 contrast, treatment with calyculin A, an inhibitor of protein phosphatases 1 and 2A that are
563 responsible for the main phosphatase activity in presynaptic terminals under basal and
564 depolarising conditions, failed to prevent Amph1-S293 dephosphorylation (Figure 8C).
565 Additionally, we examined the impact of electrical field stimulation, during which neurons
566 were stimulated with 300 APs at 10 Hz or 400 APs at 40 Hz in the presence or absence of the
567 antagonists AP5 and CNQX (which prevent postsynaptic activity or recurrent spontaneous
568 activity). We observed that Amph1-S293 was dephosphorylated after stimulation at both
569 frequencies (Figure 8D). Furthermore, the phosphorylation profile of Amph1-S293 was similar
570 to that of pDyn1-S774, an established phosphorylation site that undergoes calcineurin- and
571 activity-dependent dephosphorylation (Liu et al., 1994; Tan et al., 2003; Clayton et al., 2009).
572 Overall, these findings suggest that Amph1-S293 undergoes calcineurin-mediated
573 dephosphorylation linked to neuronal activity at the presynapse.

574

To assess whether Amph1-S293 is a CDKL5 substrate, WT and CDKL5 KO neuronal cultures were stimulated with 50 mM KCl and allowed to repolarise for different periods of increased duration to determine whether the absence of CDKL5 impacted on rephosphorylation of this residue (Figure 9B). KCl stimulation was employed to ensure complete dephosphorylation of S293, providing the widest possible dynamic range to visualise changes in its rephosphorylation. A phospho-antibody against the established endogenous CDKL5 substrate microtubule-associated protein 1S (MAP1S)-S900 was also used as a positive control (Baltussen et al., 2018; Munoz et al., 2018). In WT neurons, Amph1-S293 was efficiently rephosphorylated within 2.5 minutes after KCl stimulation (Figure 9C). In CDKL5 KO neurons there was no significant change in the phosphorylation levels of Amph1-S293 either before, during or after the KCl stimulus when compared to WT controls (Figure 9C, Two-way ANOVA with Sidak's multiple comparison test – Overall WT vs KO $p = 0.5341$, Rest $p = 0.9332$, KCl $p > 0.9999$, 2.5 min $p = 0.9864$, 5 min $p = 0.9990$, 10 min $p = 0.5856$). In contrast, phosphorylation of MAP1S-S900 was eliminated in CDKL5 KO neurons in all conditions. This supports the conclusion that Amph1-S293 is not directly phosphorylated by CDKL5 *in vivo* and, therefore, this phospho-site does not play a significant role in the slowing of SV endocytosis due to CDKL5 deficiency.

Amph1-S293 is phosphorylated independently of CDKL5 at the presynapse

The unaltered phosphorylation levels of Amph1-S293 in the absence of CDKL5 indicates that another protein kinase is responsible for its phosphorylation *in vivo*. However, it is also possible that a different protein kinase substitutes for CDKL5 activity in CDKL5 KO neurons. A

number of early studies showed that there are two protein kinases that phosphorylate Amph1-S293 *in vitro* in addition to CDKL5, including dual-specificity tyrosine phosphorylation-regulated kinase 1A (Dyrk1A) (Murakami et al., 2006) and mitogen-activated protein kinase (MAPK) (Shang et al., 2004), whereas cyclin-dependent kinase 5 (Cdk5) (Floyd et al., 2001; Liang et al., 2007) is also reported as an Amph1 kinase in mature neurons. In an attempt to unmask any potential phosphorylation of Amph1-S293 and to determine whether other protein kinases may substitute for CDKL5 in its absence, we treated WT and CDKL5 KO neurons with a cocktail of protein kinase inhibitors, including epigallocatechin gallate (EGCG), PD98059, and roscovitine to simultaneously eliminate the kinase activity of Dyrk1A, MAPK, and Cdk5, respectively (Figure 9D). KCl-induced depolarisation of WT and CDKL5 KO neurons was followed by repolarisation for 10 min (Figure 9E). We revealed that the phosphorylation levels of pAmph1-S293 were not altered between genotypes when normalised to total Amph1, as previously observed (Figure 9F, Two-way ANOVA with Sidak's multiple comparison test – Overall WT vs KO $p = 0.8115$, Rest DMSO WT vs KO $p = 0.9977$, KCl DMSO WT vs KO $p = 0.9999$, Repol DMSO WT vs KO $p = 0.9967$, Rest inhibitors WT vs KO $p = 0.9094$, KCl inhibitors WT vs KO $p > 0.9999$, Repol inhibitors WT vs KO $p = 0.9624$). Moreover, the cocktail of kinase inhibitors abolished the rephosphorylation of pAmph1-S293 post-stimulation, indicating that kinases other than CDKL5 phosphorylate this residue in WT neurons and the contribution of CDKL5 to its phosphorylation is minor, if any. Importantly, the unaltered phosphorylation of the endogenous CDKL5 substrate pMAP1S-S900 (Baltussen et al., 2018; Munoz et al., 2018) in the presence of inhibitors excludes the possibility these inhibitors to act on CDKL5. Collectively, these data suggest that at least one presynaptic kinase other than CDKL5 phosphorylates pAmph1-S293 at hippocampal neurons.

Discussion

CDD is emerging as a prominent monogenic neurodevelopmental and epileptic encephalopathy, therefore determining the key biological roles of CDKL5 will be vital in developing targeted therapies. In this work, we reveal the first direct role for CDKL5 at the presynapse, in supporting optimal SV regeneration. This requirement was specific to SV regeneration, with no other aspects of the SV life cycle impacted by the absence of the kinase. This defect in CDKL5 KO neurons was stimulus-independent, suggesting CDKL5 is required for facilitation of this process. Importantly, CDKL5 protein kinase activity was both necessary and sufficient for this role, suggesting that CDKL5-dependent phosphorylation performs a fundamental role in facilitating SV turnover during neuronal activity.

A number of postsynaptic defects has been observed in a series of CDKL5 KO model systems, such as increased (Okuda et al., 2017; Yennawar et al., 2019) or decreased (Della Sala et al., 2016) long-term potentiation, altered dendritic morphology/dynamics (Amendola et al., 2014; Della Sala et al., 2016; Tang et al., 2017; Terzic et al., 2021), upregulated NMDA receptor number (Okuda et al., 2017; Tang et al., 2019; Terzic et al., 2021) and a shift in AMPA receptor subunit composition (Yennawar et al., 2019). Furthermore, a number of studies have suggested that loss of CDKL5 impacts synapse numbers in specific brain regions. Alterations in synapse number have been proposed to modulate the frequency of miniature events in systems where CDKL5 is absent (Ricciardi et al., 2012; Della Sala et al., 2016). However, in our primary neuronal culture system, we observe no obvious change in synapse number via staining with the presynaptic marker SV2A. Our study takes advantage of a novel rodent system to model CDD, a CDKL5 KO rat. A full characterisation of the electrophysiological and behavioural phenotypes of the CDKL5 rat model is described elsewhere (de Oliveira et al.,

643 2022), however similarly to other constitutive CDKL5 KO models, they do not display overt
644 seizure activity. Hippocampal brain slices from this model system do display reduced mEPSC
645 frequency with no apparent decrease in synapse number (de Oliveira et al., 2022), suggesting
646 that this defect may be linked to dysfunctional SV regeneration rather than less available
647 synapses. Dysfunction in SV regeneration in CDKL5 KO neurons was apparent across a wide
648 range of stimulus intensities, revealing an intrinsic defect in this process. How this defect
649 manifests with respect to circuit function is a matter of active investigation, however one
650 would predict that circuits which fire at higher activity may be disproportionately impacted
651 by inefficient SV regeneration.

652 We revealed that the kinase activity of CDKL5 is necessary and sufficient for its role in SV
653 regeneration. This was achieved via use of structural/patient mutations and expression of
654 isolated domains in molecular replacement studies. The K42R mutant is a *bona fide* kinase
655 dead protein since it fails to bind ATP and phosphorylate targets *in vitro* (Lin et al., 2005). The
656 patient mutation R178P (Elia et al., 2008; Nemos et al., 2009) is also assumed to be kinase
657 dead since a similar patient mutation (R178W) abolished kinase activity *in vitro* (Munoz et al.,
658 2018). However the kinase activity of this specific mutant still has to be directly investigated.
659 The ability of the isolated CDKL5 kinase domain to fully restore presynaptic function was
660 surprising, suggesting that the unstructured C-terminus was dispensable for SV regeneration.
661 Furthermore, this region did not influence CDKL5 localisation and/or substrate recognition,
662 indicating additional research is required to elucidate its biological functionality *in vivo*.
663 Importantly, overexpression of full-length protein did not affect SV regeneration, suggesting
664 increased gene dosage is not deleterious to presynaptic function. Our findings offer
665 preliminary evidence encouraging prospective studies on *in vivo* experimental models that
666 could assess the isolated kinase domain as a gene therapy tool, since this truncated version

667 will facilitate packaging inside viral delivery vectors that have limited space. The potential of
668 this strategy to have therapeutic benefits in individuals with CDD is supported by studies
669 where re-expression of the CDKL5 gene in KO mice reversed a cohort of cell, circuit and
670 behavioural phenotypes (Terzic et al., 2021). The finding that CDD appears to be a disorder of
671 neuromaintenance and not neurodevelopment (Kind and Bird, 2021), provides support that
672 expression of the CDKL5 kinase domain later in life may restore specific aspects of brain
673 function.

674 We also revealed that S293 on Amph1 is not the CDKL5 substrate that controls SV
675 regeneration. This site was an excellent candidate, since it was situated within a CDKL5
676 consensus sequence, is phosphorylated by the kinase *in vitro* (Sekiguchi et al., 2013; Katayama
677 et al., 2015) and is the dominant *in vivo* site on Amph1 (Craft et al., 2008). Furthermore, this
678 site is dephosphorylated during neuronal activity (Murakami et al., 2006; Craft et al., 2008)
679 and its phosphorylation status controls interactions with the endocytosis protein endophilin
680 (Murakami et al., 2006; Sekiguchi et al., 2013). Finally, deficiency of Amph1 results in
681 occurrence of irreversible seizures in mice (Di Paolo et al., 2002). However, a phospho-specific
682 antibody against S293 revealed no change in its phosphorylation status in CDKL5 KO neurons.
683 A series of *in vitro* studies have identified other candidate protein kinases that could
684 phosphorylate this site (Floyd et al., 2001; Shang et al., 2004; Murakami et al., 2006; Liang et
685 al., 2007). An inhibitor cocktail containing antagonists of these protein kinases abolished
686 rephosphorylation of Amph1 S293 in both WT and CDKL5 KO neurons, suggesting that these
687 protein kinases do not substitute for CDKL5 in its absence. Given the interplay between CDKL5
688 and Dyrk1A (Oi et al., 2017; Trovo et al., 2020), we also excluded the possibility that CDKL5
689 loss may influence the phosphorylation of Amph1-S293 by Dyrk1A. The identity of the protein
690 kinase that rephosphorylates S293 is still therefore undetermined, however it is clear that its

691 phosphorylation does not mediate CDKL5-dependent effects on SV regeneration. The identity
692 of the presynaptic CDKL5 substrate(s) is currently under investigation.

693 One interesting observation was that the impact of loss of CDKL5 function on SV regeneration
694 appeared to reduce with increasing stimulus frequencies. Remarkably, CDKL5 is not the only
695 kinase of the CMGC (named after the initials of some member kinases) group that has been
696 reported to behave in a frequency-dependent manner. For example, overexpression of
697 Dyrk1A results in more profound SV endocytosis delay following low rather than high
698 frequencies in hippocampal neurons (Kim et al., 2010). This is an intriguing observation, since
699 defects in SV endocytosis are typically exacerbated with increased stimulus intensities (Zhao
700 et al., 2014; McAdam et al., 2020). Since GABAergic neurons usually fire at higher frequencies
701 (Bartos et al., 2007), this suggests that excitatory neurotransmission may be
702 disproportionately affected by the absence of CDKL5. Recent studies in conditional CDKL5 KO
703 models provide some support to this hypothesis. For example, selective deletion of CDKL5 in
704 inhibitory interneurons increases mEPSC, but not mIPSC frequency (Tang et al., 2019).
705 Furthermore, conditional KO of CDKL5 in mouse excitatory neurons resulted in overt seizure
706 phenotypes (with increased mEPSCs, but not mIPSCs), whereas the equivalent deletion in
707 inhibitory neurons had little effect (Wang et al., 2021). Therefore, there appears to be a
708 complex relationship between loss of CDKL5 function when examined at the level of intact
709 brain circuits. Consequently, it may be too soon to predict how defects in presynaptic SV
710 regeneration culminate in both global and specific circuit dysfunction and ultimately seizure
711 activity in individuals with CDD.

712 In summary, we have identified a key presynaptic role for CDKL5 in neurotransmission and
713 potentially circuit and brain function. It will be critical to determine the molecular target(s) of

714 this kinase within this specialised subcellular region to determine the extent that presynaptic

715 dysfunction underpins this neurodevelopmental and epileptic encephalopathy.

Author Contributions

Conceptualization, PCK, MAC; Methodology CK, ECD, MAC; Data analysis, CK; Visualisation, CK; Investigation, CK, DI, MAC; Resources, PCK; Writing, CK, MAC; Funding Acquisition, PCK, MAC.

References

Amendola E, Zhan Y, Mattucci C, Castroflorio E, Calcagno E, Fuchs C, Lonetti G, Silingardi D, Vyssotski AL, Farley D, Ciani E, Pizzorusso T, Giustetto M, Gross CT (2014) Mapping pathological phenotypes in a mouse model of CDKL5 disorder. PLoS One 9:e91613.

Atluri PP, Ryan TA (2006) The kinetics of synaptic vesicle reacidification at hippocampal nerve terminals. J Neurosci 26:2313-2320.

Baker K et al. (2018) SYT1-associated neurodevelopmental disorder: a case series. Brain 141:2576-2591.

Baltussen LL, Negraes PD, Silvestre M, Claxton S, Moeskops M, Christodoulou E, Flynn HR, Snijders AP, Muotri AR, Ultanir SK (2018) Chemical genetic identification of CDKL5 substrates reveals its role in neuronal microtubule dynamics. EMBO J 37:e99763.

Bartos M, Vida I, Jonas P (2007) Synaptic mechanisms of synchronized gamma oscillations in inhibitory interneuron networks. Nat Rev Neurosci 8:45-56.

Bauerfeind R, Takei K, De Camilli P (1997) Amphiphysin I is associated with coated endocytic intermediates and undergoes stimulation-dependent dephosphorylation in nerve terminals. J Biol Chem 272:30984-30992.

Boumil RM, Letts VA, Roberts MC, Lenz C, Mahaffey CL, Zhang ZW, Moser T, Frankel WN (2010) A missense mutation in a highly conserved alternate exon of dynamin-1 causes epilepsy in fitful mice. PLoS Genet 6:e1001046.

Clayton EL, Anggono V, Smillie KJ, Chau N, Robinson PJ, Cousin MA (2009) The phospho-dependent dynamin-syndapin interaction triggers activity-dependent bulk endocytosis of synaptic vesicles. J Neurosci 29:7706-7717.

Clayton EL, Sue N, Smillie KJ, O'Leary T, Bache N, Cheung G, Cole AR, Wyllie DJ, Sutherland C, Robinson PJ, Cousin MA (2010) Dynamin I phosphorylation by GSK3 controls activity-dependent bulk endocytosis of synaptic vesicles. Nat Neurosci 13:845-851.

Cousin MA (2017) Integration of Synaptic Vesicle Cargo Retrieval with Endocytosis at Central Nerve Terminals. Front Cell Neurosci 11:234.

Cousin MA, Robinson PJ (2001) The dephosphins: dephosphorylation by calcineurin triggers synaptic vesicle endocytosis. Trends Neurosci 24:659-665.

Craft GE, Graham ME, Bache N, Larsen MR, Robinson PJ (2008) The in vivo phosphorylation sites in multiple isoforms of amphiphysin I from rat brain nerve terminals. Mol Cell Proteomics 7:1146-1161.

de Oliveira LS, O'Leary H, Nawaz S, Loureiro R, Davenport E, Baxter P, Dando O, Perkins E, Booker S, Hardingham G, Cousin M, Chattarji S, Benke T, Wyllie D, Kind P (2022) Enhanced hippocampal LTP but typical NMDA receptor and AMPA receptor function in a novel rat model of CDKL5 deficiency disorder. bioRxiv:2022.2006.2029.497927.

Della Sala G, Putignano E, Chelini G, Melani R, Calcagno E, Michele Ratto G, Amendola E, Gross CT, Giustetto M, Pizzorusso T (2016) Dendritic Spine Instability in a Mouse Model of CDKL5 Disorder Is Rescued by Insulin-like Growth Factor 1. Biol Psychiatry 80:302-311.

Dhindsa RS, Bradrick SS, Yao X, Heinzen EL, Petrovski S, Krueger BJ, Johnson MR, Frankel WN, Petrou S, Boumil RM, Goldstein DB (2015) Epileptic encephalopathy-causing mutations in DNM1 impair synaptic vesicle endocytosis. Neurol Genet 1:e4.

Di Paolo G, Sankaranarayanan S, Wenk MR, Daniell L, Perucco E, Caldarone BJ, Flavell R, Picciotto MR, Ryan TA, Cremona O, De Camilli P (2002) Decreased synaptic vesicle recycling efficiency and cognitive deficits in amphiphysin 1 knockout mice. Neuron 33:789-804.

Egashira Y, Takase M, Takamori S (2015) Monitoring of vacuolar-type H+ ATPase-mediated proton influx into synaptic vesicles. J Neurosci 35:3701-3710.

Elia M, Falco M, Ferri R, Spalletta A, Bottitta M, Calabrese G, Carotenuto M, Musumeci SA, Lo Giudice M, Fichera M (2008) CDKL5 mutations in boys with severe encephalopathy and early-onset intractable epilepsy. Neurology 71:997-999.

Fassio A et al. (2018) De novo mutations of the ATP6V1A gene cause developmental encephalopathy with epilepsy. Brain 141:1703-1718.

Fehr S, Wilson M, Downs J, Williams S, Murgia A, Sartori S, Vecchi M, Ho G, Polli R, Psoni S, Bao X, de Klerk N, Leonard H, Christodoulou J (2013) The CDKL5 disorder is an independent clinical entity associated with early-onset encephalopathy. Eur J Hum Genet 21:266-273.

Ferreira APA, Casamento A, Carrillo Roas S, Halff EF, Panambalana J, Subramaniam S, Schutzenhofer K, Chan Wah Hak L, McGourty K, Thalassinos K, Kittler JT, Martinvalet D, Boucrot E (2021) Cdk5 and GSK3beta inhibit fast endophilin-mediated endocytosis. Nat Commun 12:2424.

Floyd S, Porro EB, Slepnev VI, Ochoa GC, Tsai LH, De Camilli P (2001) Amphiphysin 1 binds the cyclin-dependent kinase (cdk) 5 regulatory subunit p35 and is phosphorylated by cdk5 and cdc2. J Biol Chem 276:8104-8110.

Gordon SL, Cousin MA (2013) X-linked intellectual disability-associated mutations in synaptophysin disrupt synaptobrevin II retrieval. J Neurosci 33:13695-13700.

Gordon SL, Leube RE, Cousin MA (2011) Synaptophysin is required for synaptobrevin retrieval during synaptic vesicle endocytosis. J Neurosci 31:14032-14036.

Granseth B, Odermatt B, Royle SJ, Lagnado L (2006) Clathrin-mediated endocytosis is the dominant mechanism of vesicle retrieval at hippocampal synapses. Neuron 51:773-786.

792 Hector RD, Kalscheuer VM, Hennig F, Leonard H, Downs J, Clarke A, Benke TA, Armstrong J,
793 Pineda M, Bailey MES, Cobb SR (2017) CDKL5 variants: Improving our understanding
794 of a rare neurologic disorder. Neurol Genet 3:e200.

795 Huttner WB, Schiebler W, Greengard P, De Camilli P (1983) Synapsin I (protein I), a nerve
796 terminal-specific phosphoprotein. III. Its association with synaptic vesicles studied in
797 a highly purified synaptic vesicle preparation. J Cell Biol 96:1374-1388.

798 Jiang Z, Gong T, Wei H (2020) CDKL5 promotes proliferation, migration, and
799 chemotherapeutic drug resistance of glioma cells via activation of the PI3K/AKT
800 signaling pathway. FEBS Open Bio 10:268-277.

801 Kapur JN, Sahoo PK, Wong AKC (1985) A New Method for Gray-Level Picture Thresholding
802 Using the Entropy of the Histogram. Comput Vision Graph 29:273-285.

803 Katayama S, Sueyoshi N, Kameshita I (2015) Critical Determinants of Substrate Recognition by
804 Cyclin-Dependent Kinase-like 5 (CDKL5). Biochemistry 54:2975-2987.

805 Kilstrup-Nielsen C, Rusconi L, La Montanara P, Ciceri D, Bergo A, Bedogni F, Landsberger N
806 (2012) What we know and would like to know about CDKL5 and its involvement in
807 epileptic encephalopathy. Neural Plast 2012:728267.

808 Kim Y, Park J, Song WJ, Chang S (2010) Overexpression of Dyrk1A causes the defects in
809 synaptic vesicle endocytosis. Neurosignals 18:164-172.

810 Kind PC, Bird A (2021) CDKL5 deficiency disorder: a pathophysiology of neural maintenance. J
811 Clin Invest 131.

812 Koch D et al. (2011) Proper synaptic vesicle formation and neuronal network activity critically
813 rely on syndapin I. EMBO J 30:4955-4969.

814 Liang S, Wei FY, Wu YM, Tanabe K, Abe T, Oda Y, Yoshida Y, Yamada H, Matsui H, Tomizawa
815 K, Takei K (2007) Major Cdk5-dependent phosphorylation sites of amphiphysin 1 are
816 implicated in the regulation of the membrane binding and endocytosis. J Neurochem
817 102:1466-1476.

818 Lin C, Franco B, Rosner MR (2005) CDKL5/Stk9 kinase inactivation is associated with neuronal
819 developmental disorders. Hum Mol Genet 14:3775-3786.

820 Liu JP, Sim AT, Robinson PJ (1994) Calcineurin inhibition of dynamin I GTPase activity coupled
821 to nerve terminal depolarization. Science 265:970-973.

822 Marks B, McMahon HT (1998) Calcium triggers calcineurin-dependent synaptic vesicle
823 recycling in mammalian nerve terminals. Curr Biol 8:740-749.

824 McAdam RL, Morton A, Gordon SL, Alterman JF, Khvorova A, Cousin MA, Smillie KJ (2020) Loss
825 of huntingtin function slows synaptic vesicle endocytosis in striatal neurons from the
826 htt(Q140/Q140) mouse model of Huntington's disease. Neurobiol Dis 134:104637.

827 Micheva KD, Ramjaun AR, Kay BK, McPherson PS (1997) SH3 domain-dependent interactions
828 of endophilin with amphiphysin. FEBS Lett 414:308-312.

829 Miesenbock G, De Angelis DA, Rothman JE (1998) Visualizing secretion and synaptic
830 transmission with pH-sensitive green fluorescent proteins. Nature 394:192-195.

831 Munoz IM, Morgan ME, Peltier J, Weiland F, Gregorczyk M, Brown FC, Macartney T, Toth R,
832 Trost M, Rouse J (2018) Phosphoproteomic screening identifies physiological
833 substrates of the CDKL5 kinase. EMBO J 37:e99559.

834 Murakami N, Xie W, Lu RC, Chen-Hwang MC, Wieraszko A, Hwang YW (2006) Phosphorylation
835 of amphiphysin I by minibrain kinase/dual-specificity tyrosine phosphorylation-
836 regulated kinase, a kinase implicated in Down syndrome. J Biol Chem 281:23712-
837 23724.

838 Nawaz MS, Giarda E, Bedogni F, La Montanara P, Ricciardi S, Ciceri D, Alberio T, Landsberger
839 N, Rusconi L, Kilstrup-Nielsen C (2016) CDKL5 and Shootin1 Interact and Concur in
840 Regulating Neuronal Polarization. PLoS One 11:e0148634.

841 Nemos C, Lambert L, Giuliano F, Doray B, Roubertie A, Goldenberg A, Delobel B, Layet V,
842 N'Guyen M A, Saunier A, Verneau F, Jonveaux P, Philippe C (2009) Mutational
843 spectrum of CDKL5 in early-onset encephalopathies: a study of a large collection of
844 French patients and review of the literature. Clin Genet 76:357-371.

845 Nichols RA, Suplick GR, Brown JM (1994) Calcineurin-mediated protein dephosphorylation in
846 brain nerve terminals regulates the release of glutamate. J Biol Chem 269:23817-
847 23823.

848 Oi A, Katayama S, Hatano N, Sugiyama Y, Kameshita I, Sueyoshi N (2017) Subcellular
849 distribution of cyclin-dependent kinase-like 5 (CDKL5) is regulated through
850 phosphorylation by dual specificity tyrosine-phosphorylation-regulated kinase 1A
851 (DYRK1A). Biochem Biophys Res Commun 482:239-245.

852 Okuda K, Kobayashi S, Fukaya M, Watanabe A, Murakami T, Hagiwara M, Sato T, Ueno H,
853 Ogonuki N, Komano-Inoue S, Manabe H, Yamaguchi M, Ogura A, Asahara H, Sakagami
854 H, Mizuguchi M, Manabe T, Tanaka T (2017) CDKL5 controls postsynaptic localization
855 of GluN2B-containing NMDA receptors in the hippocampus and regulates seizure
856 susceptibility. Neurobiol Dis 106:158-170.

857 Parenti I, Rabaneda LG, Schoen H, Novarino G (2020) Neurodevelopmental Disorders: From
858 Genetics to Functional Pathways. Trends Neurosci 43:608-621.

859 Ren E, Roncace V, Trazzi S, Fuchs C, Medici G, Gennaccaro L, Loi M, Galvani G, Ye K, Rimondini
860 R, Aicardi G, Ciani E (2019) Functional and Structural Impairments in the Perirhinal
861 Cortex of a Mouse Model of CDKL5 Deficiency Disorder Are Rescued by a TrkB Agonist.
862 Front Cell Neurosci 13:169.

863 Ricciardi S, Ungaro F, Hambrock M, Rademacher N, Stefanelli G, Brambilla D, Sessa A,
864 Magagnotti C, Bachi A, Giarda E, Verpelli C, Kilstrup-Nielsen C, Sala C, Kalscheuer VM,

865 Broccoli V (2012) CDKL5 ensures excitatory synapse stability by reinforcing NGL-1-
866 PSD95 interaction in the postsynaptic compartment and is impaired in patient iPSC-
867 derived neurons. Nat Cell Biol 14:911-923.

868 Rusconi L, Kilstrup-Nielsen C, Landsberger N (2011) Extrasynaptic N-methyl-D-aspartate
869 (NMDA) receptor stimulation induces cytoplasmic translocation of the CDKL5 kinase
870 and its proteasomal degradation. J Biol Chem 286:36550-36558.

871 Salpietro V et al. (2019) Mutations in the Neuronal Vesicular SNARE VAMP2 Affect Synaptic
872 Membrane Fusion and Impair Human Neurodevelopment. Am J Hum Genet 104:721-
873 730.

874 Sankaranarayanan S, Ryan TA (2000) Real-time measurements of vesicle-SNARE recycling in
875 synapses of the central nervous system. Nat Cell Biol 2:197-204.

876 Sankaranarayanan S, Ryan TA (2001) Calcium accelerates endocytosis of vSNAREs at
877 hippocampal synapses. Nat Neurosci 4:129-136.

878 Schindelin J, Arganda-Carreras I, Frise E, Kaynig V, Longair M, Pietzsch T, Preibisch S, Rueden
879 C, Saalfeld S, Schmid B, Tinevez JY, White DJ, Hartenstein V, Eliceiri K, Tomancak P,
880 Cardona A (2012) Fiji: an open-source platform for biological-image analysis. Nat
881 Methods 9:676-682.

882 Schneider CA, Rasband WS, Eliceiri KW (2012) NIH Image to ImageJ: 25 years of image analysis.
883 Nat Methods 9:671-675.

884 Schroeder E, Yuan L, Seong E, Ligon C, DeKorver N, Gurumurthy CB, Arikkath J (2019) Neuron-
885 Type Specific Loss of CDKL5 Leads to Alterations in mTOR Signaling and Synaptic
886 Markers. Mol Neurobiol 56:4151-4162.

887 Sekiguchi M, Katayama S, Hatano N, Shigeri Y, Sueyoshi N, Kameshita I (2013) Identification
888 of amphiphysin 1 as an endogenous substrate for CDKL5, a protein kinase associated
889 with X-linked neurodevelopmental disorder. Arch Biochem Biophys 535:257-267.

890 Serajee FJ, Huq AM (2015) Homozygous Mutation in Synaptic Vesicle Glycoprotein 2A Gene
891 Results in Intractable Epilepsy, Involuntary Movements, Microcephaly, and
892 Developmental and Growth Retardation. Pediatr Neurol 52:642-646 e641.

893 Shang WH, Adachi Y, Nakamura A, Copeland T, Kim SR, Kamata T (2004) Regulation of
894 amphiphysin1 by mitogen-activated protein kinase: its significance in nerve growth
895 factor receptor-mediated endocytosis. J Biol Chem 279:40890-40896.

896 Sivilia S, Mangano C, Beggiato S, Giuliani A, Torricella R, Baldassarro VA, Fernandez M,
897 Lorenzini L, Giardino L, Borelli AC, Ferraro L, Calza L (2016) CDKL5 knockout leads to
898 altered inhibitory transmission in the cerebellum of adult mice. Genes Brain Behav
899 15:491-502.

900 Smillie KJ, Cousin MA (2012) Akt/PKB controls the activity-dependent bulk endocytosis of
901 synaptic vesicles. Traffic 13:1004-1011.

902 Soykan T, Maritzen T, Haucke V (2016) Modes and mechanisms of synaptic vesicle recycling.
903 Curr Opin Neurobiol 39:17-23.

904 Tan TC, Valova VA, Malladi CS, Graham ME, Berven LA, Jupp OJ, Hansra G, McClure SJ, Sarcevic
905 B, Boadle RA, Larsen MR, Cousin MA, Robinson PJ (2003) Cdk5 is essential for synaptic
906 vesicle endocytosis. Nat Cell Biol 5:701-710.

907 Tang S, Wang IJ, Yue C, Takano H, Terzic B, Pance K, Lee JY, Cui Y, Coulter DA, Zhou Z (2017)
908 Loss of CDKL5 in Glutamatergic Neurons Disrupts Hippocampal Microcircuitry and
909 Leads to Memory Impairment in Mice. J Neurosci 37:7420-7437.

910 Tang S, Terzic B, Wang IJ, Sarmiento N, Sizov K, Cui Y, Takano H, Marsh ED, Zhou Z, Coulter DA
911 (2019) Altered NMDAR signaling underlies autistic-like features in mouse models of
912 CDKL5 deficiency disorder. Nat Commun 10:2655.

913 Terzic B, Davatolhagh MF, Ho Y, Tang S, Liu YT, Xia Z, Cui Y, Fuccillo MV, Zhou Z (2021)
914 Temporal manipulation of Cdkl5 reveals essential postdevelopmental functions and
915 reversible CDKL5 deficiency disorder-related deficits. J Clin Invest 131:e143655.

916 Thapar A, Cooper M, Rutter M (2017) Neurodevelopmental disorders. Lancet Psychiatry
917 4:339-346.

918 Thevenaz P, Ruttimann UE, Unser M (1998) A pyramid approach to subpixel registration based
919 on intensity. IEEE Trans Image Process 7:27-41.

920 Trovo L, Fuchs C, De Rosa R, Barbiero I, Tramarin M, Ciani E, Rusconi L, Kilstrup-Nielsen C
921 (2020) The green tea polyphenol epigallocatechin-3-gallate (EGCG) restores CDKL5-
922 dependent synaptic defects in vitro and in vivo. Neurobiol Dis 138:104791.

923 Wang HT, Zhu ZA, Li YY, Lou SS, Yang G, Feng X, Xu W, Huang ZL, Cheng X, Xiong ZQ (2021)
924 CDKL5 deficiency in forebrain glutamatergic neurons results in recurrent spontaneous
925 seizures. Epilepsia 62:517-528.

926 Wang IT, Allen M, Goffin D, Zhu X, Fairless AH, Brodkin ES, Siegel SJ, Marsh ED, Blendy JA,
927 Zhou Z (2012) Loss of CDKL5 disrupts kinome profile and event-related potentials
928 leading to autistic-like phenotypes in mice. Proc Natl Acad Sci U S A 109:21516-21521.

929 Wigge P, McMahon HT (1998) The amphiphysin family of proteins and their role in
930 endocytosis at the synapse. Trends Neurosci 21:339-344.

931 Wu Y, Matsui H, Tomizawa K (2009) Amphiphysin I and regulation of synaptic vesicle
932 endocytosis. Acta Med Okayama 63:305-323.

933 Yennawar M, White RS, Jensen FE (2019) AMPA Receptor Dysregulation and Therapeutic
934 Interventions in a Mouse Model of CDKL5 Deficiency Disorder. J Neurosci 39:4814-
935 4828.

936 Zhao H, Kim Y, Park J, Park D, Lee SE, Chang I, Chang S (2014) SCAMP5 plays a critical role in
937 synaptic vesicle endocytosis during high neuronal activity. J Neurosci 34:10085-10095.

Zhu YC, Li D, Wang L, Lu B, Zheng J, Zhao SL, Zeng R, Xiong ZQ (2013) Palmitoylation-dependent CDKL5-PSD-95 interaction regulates synaptic targeting of CDKL5 and dendritic spine development. Proc Natl Acad Sci U S A 110:9118-9123.

Table 1. Table of experimental *n*, *p* values and statistical tests.

Figure 1	Group	Mean ± SEM	n = # of fields of view/ N = # of neuronal preparations	Comparison	*P*	Statistical test
Fig. 1C	mCer	40.42 ± 0.88	48/4	mCer vs. Syp1-mCer	<0.0001	One-way ANOVA with Tukey's multiple comparison test
	Syp1-mCer	72.99 ± 1.55	37/4	mCer vs. mCer-CDKL5	0.0640	
	mCer-CDKL5	36.52 ± 1.22	32/4	Syp1-mCer vs. mCer-CDKL5	<0.0001	

Figure 2	Group	Mean ± SEM (Fig. 2A) or median (min - max) (Fig. 2C,D)	n = # of neuronal lysates (Fig. 2A) or neurons (Fig. 2C,D)/ N = # of neuronal preparations	Comparison	*P*	Statistical test
Fig. 2A	CDKL5 WT	1.00 ± 0.10	4/4	WT vs. KO	<0.0001	Unpaired two-tailed *t* test
	CDKL5 KO	0.02 ± 0.01	4/4			
	CHC WT	1.00 ± 0.09	4/4		0.4921	
	CHC KO	0.85 ± 0.19	4/4			
	Dyn1 WT	1.00 ± 0.12	4/4		0.1808	
	Dyn1 KO	0.79 ± 0.06	4/4			
	Syndapin 1 WT	1.00 ± 0.25	4/4		0.6711	
	Syndapin 1 KO	0.87 ± 0.13	4/4			
	Endophilin A1 WT	1.00 ± 0.28	4/4		0.4505	
	Endophilin A1 KO	0.74 ± 0.16	4/4			
	VGLUT1 WT	1.00 ± 0.07	4/4		0.9899	
	VGLUT1 KO	0.10 ± 0.21	4/4			
	ATP6V1B2 WT	1.00 ± 0.12	4/4		0.2114	
	ATP6V1B2 KO	0.83 ± 0.04	4/4			
	Syp1 WT	1.00 ± 0.07	4/4		0.0592	
	Syp1 KO	1.33 ± 0.12	4/4			
	pAkt-S473 WT	1.00 ± 0.07	4/4		0.6186	
	pAkt-S473 KO	1.05 ± 0.05	4/4			
	pGSK3α/β-S9/S21 WT	1.00 ± 0.08	4/4		0.2271	
	pGSK3α/β-S9/S21 KO	1.21 ± 0.13	4/4			
Fig. 2C	$SV2A^+$ WT	19.67 (4.33 - 43.33)	144/4	WT vs. KO	0.2854	Mann Whitney two-tailed test
	$SV2A^+$ KO	19.00 (4.33 - 45.00)	142/4			
Fig. 2D	$VGLUT1^+$ WT	22.83 (8.00 - 45.67)	144/4	WT vs. KO	0.2302	Mann Whitney two-tailed test
	$VGLUT1^+$ KO	21.50 (9.67 - 41.67)	142/4			

Figure 3	Group	Mean ± SEM	n = # of coverslips/ N = # of neuronal preparations	Comparison	*P*	Statistical test
Fig. 3C	WT	0.44 ± 0.02	12/4	WT vs. KO	0.8932	Unpaired two-tailed *t* test
	KO	0.45 ± 0.02	12/4			
Fig. 3D	WT	0.16 ± 0.04	12/4	WT vs. KO	0.0022	Unpaired two-tailed *t* test
	KO	0.36 ± 0.04	12/4			
Fig. 3F	WT	0.49 ± 0.02	13/4	WT vs. KO	0.3025	

	KO	0.53 ± 0.03	14/4			Unpaired two-tailed *t* test
Fig. 3G	WT	0.22 ± 0.03	13/4	WT vs. KO	0.0065	Unpaired two-tailed *t* test
	KO	0.32 ± 0.02	14/4			
Fig. 3I	WT	0.45 ± 0.03	12/4	WT vs. KO	0.6015	Unpaired two-tailed *t* test
	KO	0.48 ± 0.05	13/4			
Fig. 3J	WT	0.15 ± 0.03	12/4	WT vs. KO	0.0442	Unpaired two-tailed *t* test
	KO	0.24 ± 0.02	13/4			
Fig 3L	WT	0.19 ± 0.02	15/2	WT vs. KO	0.3680	Unpaired two-tailed *t* test
	KO	0.16 ± 0.02	15/2			
Fig 3M	WT	-0.23 ± 0.09	15/2	WT vs. KO	0.0409	Unpaired two-tailed *t* test
	KO	0.03 ± 0.08	15/2			

Figure 4	**Group**	**Mean ± SEM**	**n = # of coverslips/ N = # of neuronal preparations**	**Comparison**	***P***	**Statistical test**
Fig. 4B	WT	2.41 ± 0.14	17/4	WT vs. KO	0.3494	Unpaired two-tailed *t* test
	KO	2.63 ± 0.18	17/4			
Fig. 4C	WT	0.39 ± 0.01	17/4	WT vs. KO	0.3477	Unpaired two-tailed *t* test
	KO	0.41 ± 0.01	17/4			
Fig. 4E	WT	0.52 ± 0.04	16/3	WT vs. KO	0.5061	Unpaired two-tailed *t* test
	KO	0.48 ± 0.03	13/3			

Figure 5	**Group**		**Mean ± SEM**	**n = # of coverslips/ N = # of neuronal preparations**	**Comparison**	***P***	**Statistical test**
Fig. 5B	WT	Empty	0.04 ± 0.03	15/4	WT Empty vs. KO Empty WT Empty vs. WT-CDKL5 WT Empty vs. KO-CDKL5 KO Empty vs. WT-CDKL5 KO Empty vs. KO-CDKL5 WT-CDKL5 vs. KO-CDKL5	0.0419 0.9644 0.9956 0.0134 0.0229 0.9947	Two-way ANOVA with Tukey's multiple comparison test
		CDKL5	0.01 ± 0.02	14/4			
	KO	Empty	0.17 ± 0.04	16/4			
		CDKL5	0.03 ± 0.04	15/4			
Fig. 5D	WT	Empty	0.10 ± 0.02	20/5	WT Empty vs. KO Empty WT Empty vs. WT-CDKL5 WT Empty vs. KO-CDKL5 KO Empty vs. WT-CDKL5 KO Empty vs. KO-CDKL5 WT-CDKL5 vs. KO-CDKL5	0.0158 0.9982 0.5756 0.0317 0.3186 0.7013	Two-way ANOVA with Tukey's multiple comparison test
		CDKL5	0.10 ± 0.02	18/5			
	KO	Empty	0.20 ± 0.03	21/5			
		CDKL5	0.14 ± 0.02	19/5			

Figure 6	**Group**	**Mean ± SEM**	**n = # of coverslips/ N = # of neuronal preparations**	**Comparison**	***P***	**Statistical test**
Fig. 6C	KO	0.26 ± 0.01	17/4	KO vs. CDKL5 KO vs. K42R KO vs. R178P	0.0006 0.5993 0.6845	One-way ANOVA with Dunnett's multiple comparison test
	CDKL5	0.14 ± 0.02	16/4			
	K42R	0.23 ± 0.03	15/4			
	R178P	0.23 ± 0.02	15/4			
Fig. 6E	KO	0.34 ± 0.03	13/4	KO vs. CDKL5 KO vs. K42R KO vs. R178P	0.0135 0.9827 0.8653	One-way ANOVA with Dunnett's multiple comparison test
	CDKL5	0.22 ± 0.02	14/4			
	K42R	0.33 ± 0.03	13/4			
	R178P	0.31 ± 0.03	14/4			

Figure 7	Group	Median (min - max) (Fig. 7C) or mean ± SEM (Fig.7E,G)	n = # of coverslips/ N = # of neuronal preparations	Comparison	*P*	Statistical test
Fig. 7C	mCer	4.74 (1.53 - 23.67)	191/4	mCer vs. CDKL5 mCer vs. Δkinase CDKL5 vs. Δkinase	<0.0001 <0.0001 0.0038	Kruskal-Wallis test with Dunn's multiple comparison test
	CDKL5	6.96 (1.81 - 46.13)	149/4			
	Δkinase	9.34 (2.59 - 49.79)	71/4			
Fig. 7E	KO	0.19 ± 0.02	13/4	KO vs. CDKL5 KO vs. ΔC KO vs. Δkinase	0.0044 0.0010 0.4857	One-way ANOVA with Dunnett's multiple comparison test
	CDKL5	0.07 ± 0.03	11/4			
	ΔC	0.07 ± 0.02	18/4			
	Δkinase	0.15 ± 0.02	15/4			
Fig. 7G	KO	0.25 ± 0.02	11/3	KO vs. CDKL5 KO vs. ΔC KO vs. Δkinase	0.0331 0.0281 0.9334	One-way ANOVA with Dunnett's multiple comparison test
	CDKL5	0.17 ± 0.02	10/3			
	ΔC	0.16 ± 0.02	10/3			
	Δkinase	0.26 ± 0.02	10/3			

Figure 9	Group		Mean ± SEM	n = # of coverslips/ N = # of neuronal preparations	Comparison	*p*	Statistical test
Fig. 9C	WT	Rest	1.00 ± 0.09	3/3	WT vs. KO overall	0.5341	Two-way ANOVA with Sidak's multiple comparison test
		KCl	0.03 ± 0.02	3/3			
		Repol. 2.5 min	0.80 ± 0.23	3/3			
		Repol. 5 min	0.81 ± 0.04	3/3			
		Repol. 10 min	0.76 ± 0.21	3/3			
	KO	Rest	0.85 ± 0.05	3/3	WT vs. KO Rest WT vs. KO KCl WT vs. KO Repol. 2.5 min WT vs. KO Repol. 5 min WT vs. KO Repol. 10 min	0.9332 >0.9999 0.9864 0.9990 0.5856	
		KCl	0.06 ± 0.03	3/3			
		Repol. 2.5 min	0.69 ± 0.06	3/3			
		Repol. 5 min	0.75 ± 0.06	3/3			
		Repol. 10 min	1.03 ± 0.22	3/3			
Fig. 9F	WT	DMSO-Rest	1.00 ± 0.16	3/3	WT vs. KO overall	0.8115	Two-way ANOVA with Sidak's multiple comparison test
		DMSO-KCl	0.17 ± 0.02	3/3			
		DMSO-Repol.	0.79 ± 0.03	3/3			
		Inhibitors-Rest	0.69 ± 0.06	3/3			
		Inhibitors-KCl	0.05 ± 0.03	3/3			
		Inhibitors-Repol.	0.12 ± 0.05	3/3			
	KO	DMSO-Rest	0.94 ± 0.13	3/3	WT vs. KO DMSO-Rest WT vs. KO DMSO-KCl WT vs. KO DMSO-Repol. WT vs. KO Inhibitors-Rest WT vs. KO Inhibitors-KCl WT vs. KO Inhibitors-Repol.	0.9977 0.9999 0.9967 0.9094 >0.9999 0.9624	
		DMSO-KCl	0.13 ± 0.06	3/3			
		DMSO-Repol.	0.85 ± 0.13	3/3			
		Inhibitors-Rest	0.81 ± 0.10	3/3			
		Inhibitors-KCl	0.05 ± 0.03	3/3			
		Inhibitors-Repol.	0.02 ± 0.01	3/3			

960

961

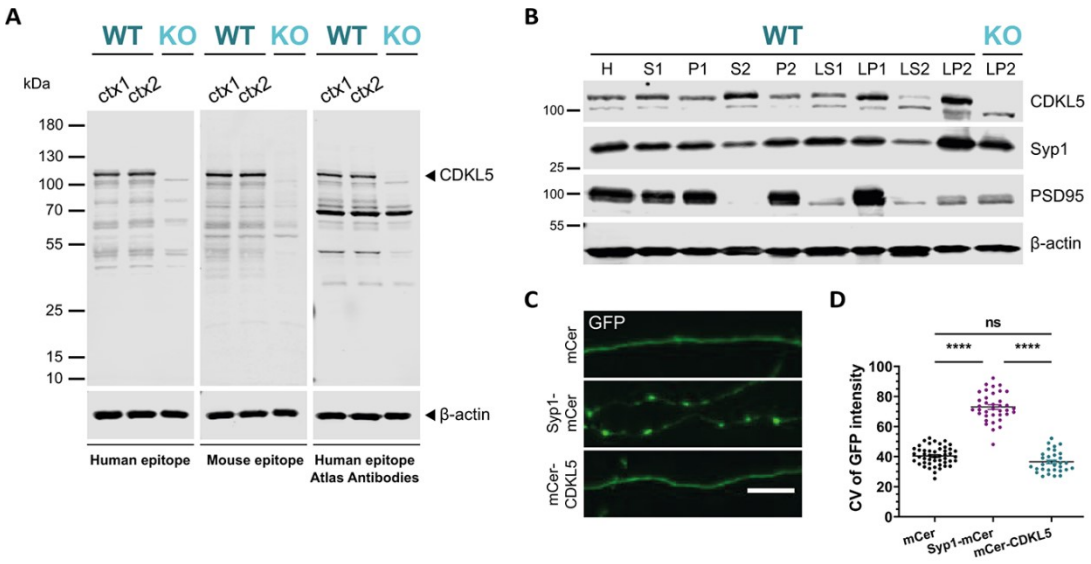

969

970 **Figure 1. CDKL5 is present at nerve terminals.** (*A*) CDKL5 protein is absent from *Cdkl5* KO LE
971 rats. Immunoblots of cortical lysates generated from WT and CDKL5 KO animals at P14 using
972 three different antibodies against CDKL5. Two antibodies were raised against a human (aa
973 350-650) and a mouse (aa 300-600) epitope on CDKL5, respectively, whereas the Atlas CDKL5
974 antibody was tested as a commercially available alternative. CDKL5 is detected as a 110-kDa
975 band that is absent from KO tissues. All three antibodies detect numerous non-specific bands
976 observed in both WT and CDKL5 KO tissues. In all cases, β-actin was used as a loading control.
977 (*B*) Subcellular fractionation of adult rat brain for the crude purification of a synaptosomal
978 (P2) and an SV (LP2) fraction and fractions representing other subcellular compartments (H,
979 homogenate; P1, tissue debris, nuclei, and large myelin fragments; S2, microsomes,
980 mitochondria, and synaptosomes; LP1, synaptic membrane, mitochondria, and myelin
981 fragments; LS2, synaptosomal cytoplasm). An LP2 fraction from an adult CDKL5 KO rat brain
982 was also generated. CDKL5 is enriched in the LP2 fraction (top band; 110 KDa). Synaptophysin
983 1 (Syp1) and postsynaptic density 95 (PSD95) were used as pre- and postsynaptic markers,
984 respectively, and β-actin as loading control. (*C*) Mouse hippocampal neurons were
985 transfected with either mCer, Syp1-mCer or mCer-CDKL5 at 8-9 DIV, fixed at 15 DIV, and

986 stained for GFP. Examples of axonal segments of > 15 µm that were selected for coefficient
987 of variation (CV) analysis are displayed. Scale bar, 5 µm. (*D*) The distribution pattern of CDKL5
988 was assessed by CV analysis of GFP fluorescence intensity along multiple > 15 µm axonal
989 segments per field of view. Scatter plots indicate mean ± SEM. ns, not significant, ****$p <$
990 0.0001 by one-way ANOVA followed by Tukey's multiple comparison test. mCer $n = 48$, Syp1-
991 mCer $n = 37$, mCer-CDKL5 $n = 32$ fields of view from 4 independent preparations of neuronal
992 cultures.
993

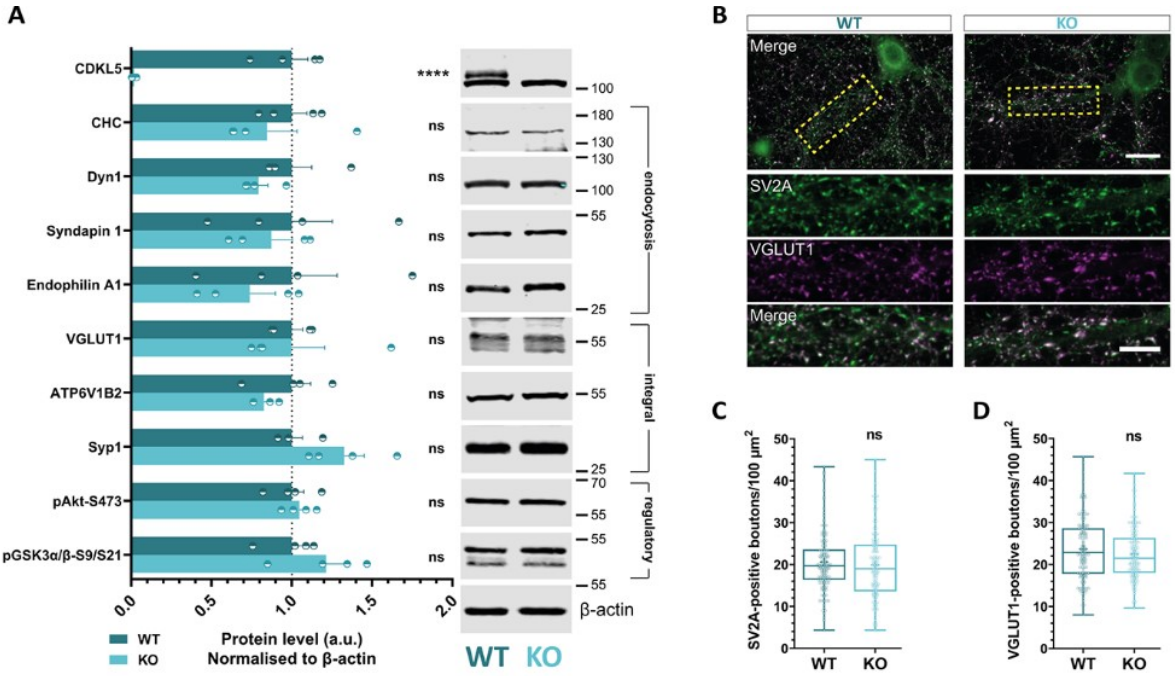

994 **Figure 2. Loss of CDKL5 does not alter presynaptic protein levels or the number of**
995 **presynaptic boutons.** (*A*) Hippocampal neuronal lysates at 14-15 DIV were analysed for
996 different presynaptic proteins, including SV endocytosis proteins, integral SV proteins, and
997 phosphoproteins regulating SV endocytosis. Quantification of the total band intensity
998 normalised to β-actin revealed no difference for any of these proteins in the absence of
999 CDKL5. Bars indicate mean ± SEM. ns, not significant, ****$p < 0.0001$ by unpaired two-tailed
1000 *t* test. WT $n = 4$, KO $n = 4$ neuronal lysates from 4 independent preparations of neuronal
1001 cultures. (*B*) Hippocampal neuronal cultures derived from WT and CDKL5 KO rats were fixed
1002 at 15 DIV and stained for the presynaptic proteins SV2A and VGLUT1. The number of positive
1003 puncta was counted in (50 x 15) µm^2 selections along dendrites (dashed yellow boxes) for
1004 both markers. Scale bar, 20 µm (neurons), 10 µm (processes). (*C*) Quantification of SV2A-
1005 positive boutons and (*D*) VGLUT1-positive boutons per 100 µm^2 along WT and CDKL5 KO
1006 dendrites. Box plots present median with IQR indicating min to max whiskers. ns, not

1007 significant by Mann Whitney two-tailed *t* test, + indicates mean value. WT *n* = 144, KO *n* = 142

1008 neurons from 3 independent preparations of neuronal cultures.

1009

1010

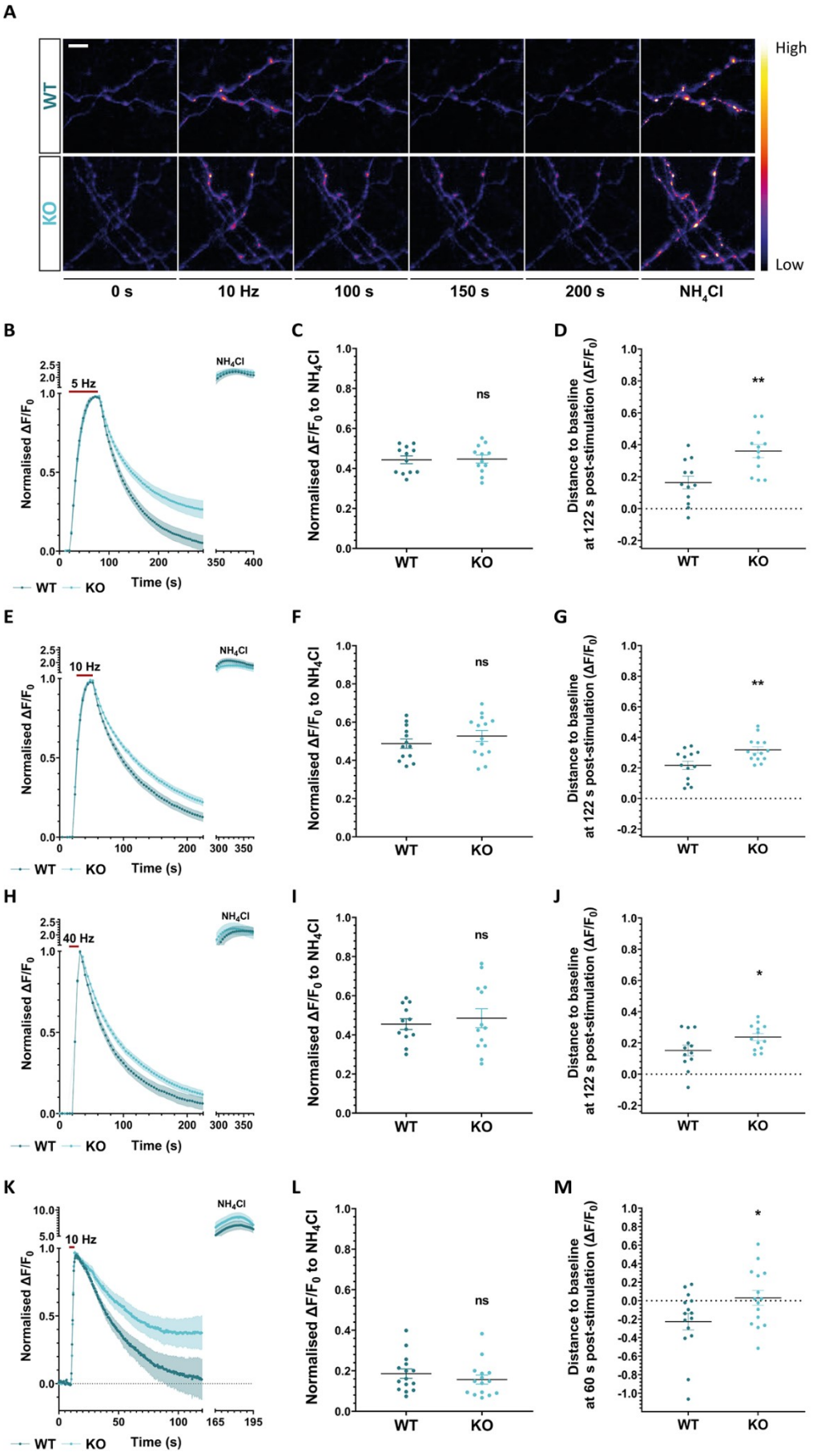
A
WT
KO
High
Low
0 s
10 Hz
100 s
150 s
200 s
NH4Cl
B
5 Hz
NH4Cl
Normalised ΔF/F0
Time (s)
WT
KO
C
Normalised ΔF/F0 to NH4Cl
ns
D
Distance to baseline at 122 s post-stimulation (ΔF/F0)
**
E
10 Hz
F
G
H
40 Hz
I
J
*
K
10 Hz
L
M
Distance to baseline at 60 s post-stimulation (ΔF/F0)

Figure 3. Loss of CDKL5 impairs the kinetics of SV endocytosis but not SV exocytosis. Primary hippocampal neurons from WT and CDKL5 KO rats were transfected with sypHy at 8-9 DIV and used at 13-14 DIV. (*A*) Example responses from sypHy-expressing axons that were subjected to 300 APs at 10 Hz and perfused with NH_4Cl solution 3 min after termination of stimulation. Representative image slices were selected from the time-course that was recorded from both WT (top) and CDKL5 KO neuronal cultures (bottom). Scale bar, 5 µm. SypHy response from neurons stimulated with either 300 APs at 5 Hz (*B*), 300 APs at 10 Hz (*E*), 400 APs at 40 Hz (*H*), or 20 APs at 10 Hz (*K*) (red bars) normalised to the stimulation peak ($\Delta F/F_0$). (*C*, *F*, *I, L*) SypHy fluorescence ($\Delta F/F_0$) at stimulation peak when total sypHy response was normalised to NH_4Cl. (*D*, *G*, *J, M*) sypHy fluorescence ($\Delta F/F_0$) measuring the distance from baseline at 122 s or 60 s post-stimulation. Scatter plots indicate mean ± SEM. ns, not significant, $*p < 0.05$, $**p < 0.01$ by unpaired two-tailed *t* test. (*B-D*) *n* = 12, KO *n* = 12 coverslips from 4 independent preparations of neuronal cultures. (*E-G*) WT *n* = 13, KO *n* = 14 coverslips from 4 independent preparations of neuronal cultures. (*H-J*) WT *n* = 12, KO *n* = 13 coverslips from 4 independent preparations of neuronal cultures. (*K-M*) WT *n* = 15, KO *n* = 15 coverslips from 2 independent preparations of neuronal cultures.

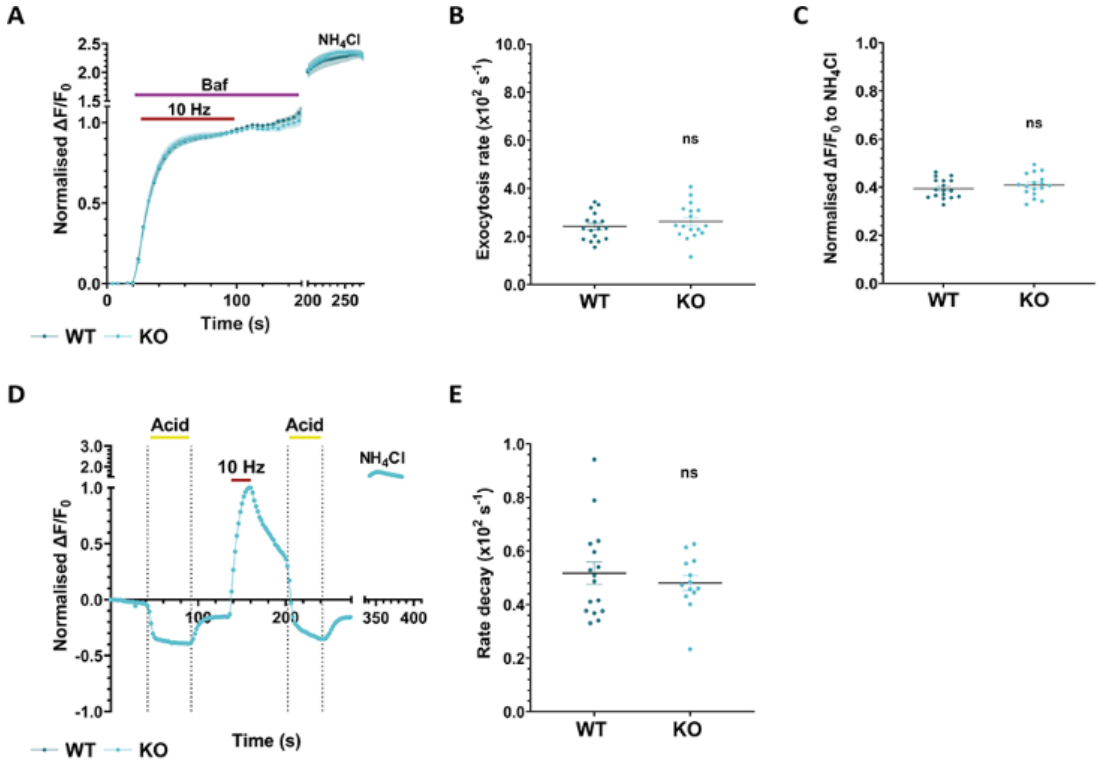

1031 **Figure 4. Loss of CDKL5 does not alter SV exocytosis rate, total pool size, or SV acidification**
1032 **rate.** Primary hippocampal neurons from WT and CDKL5 KO rats were transfected with sypHy
1033 at 8-9 DIV and used at 13-14 DIV. (*A*) sypHy response from neurons stimulated with 900 APs
1034 at 10 Hz (red bar) in the presence of 1 µM bafilomycin A1 (purple bar) normalised to the
1035 plateau. (*B*) Quantification of exocytosis rate. Scatter plots indicate mean ± SEM. ns, not
1036 significant by unpaired two-tailed *t* test. WT *n* = 17, KO *n* = 17 coverslips from 4 independent
1037 preparations of neuronal cultures. (*C*) SypHy response at plateau following perfusion with
1038 NH_4Cl. Scatter plots indicate mean ± SEM. ns, not significant by unpaired two-tailed *t* test. WT
1039 *n* = 17, KO *n* = 17 coverslips from 4 independent preparations of neuronal cultures. (*D*)
1040 Representative sypHy response from neuron stimulated with 300 APs at 10 Hz (red bar)
1041 normalised to the stimulation peak. Acidic solution was perfused both pre- and post-
1042 stimulation for 50 s and 40 s, respectively (yellow bars). (*E*) Rate decay of sypHy fluorescence
1043 measured after applying a post-stimulus acidic pulse. Scatter plots indicate mean ± SEM. ns,

not significant by unpaired two-tailed *t* test. WT *n* = 16, KO *n* = 13 coverslips from 3 independent preparations of neuronal cultures.

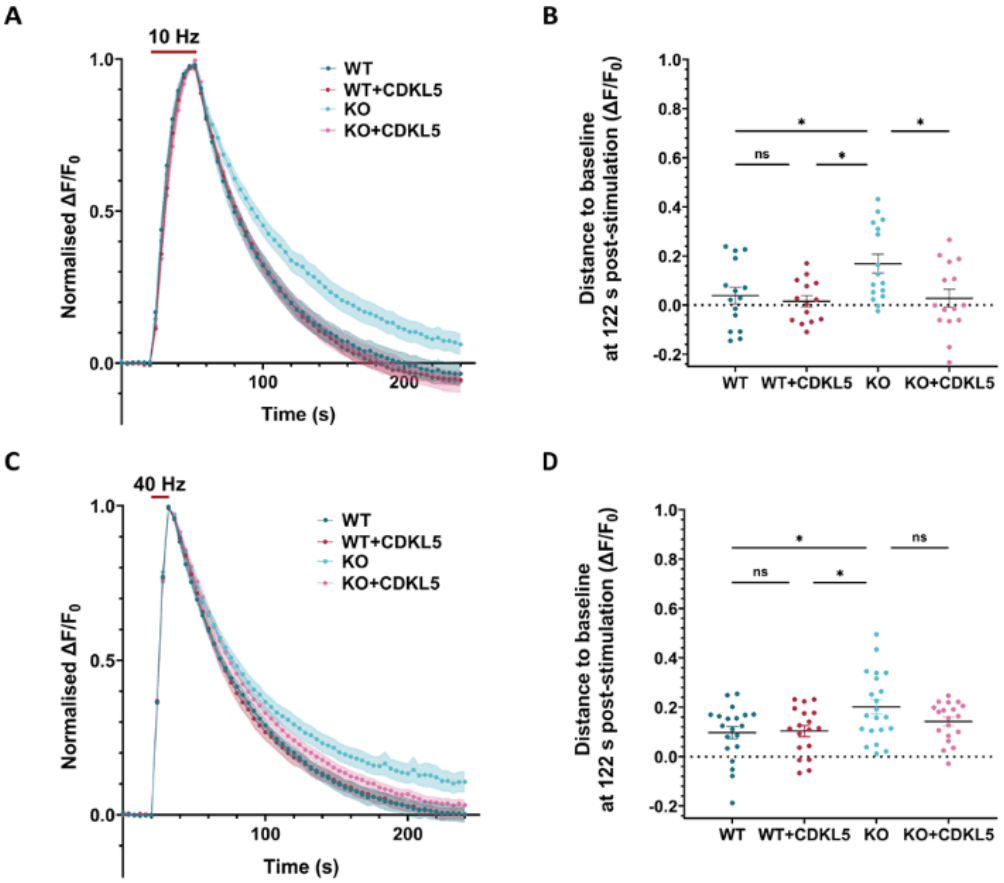

Figure 5. CDKL5 rescues the kinetics of SV endocytosis in CDKL5-deficient neurons. Primary hippocampal neurons from WT and CDKL5 KO rats were co-transfected with sypHy and mCer (WT, dark turquoise; KO, dark pink) or mCer-CDKL5 (WT+CDKL5, light turquoise; KO+CDKL5, light pink) at 8-9 DIV and used at 13-14 DIV. (*A*,*C*) sypHy response from neurons stimulated (red bar) with either 300 APs at 10 Hz (*A*) or 400 APs at 40 Hz (*C*) normalised to the stimulation peak and (*B*,*D*) sypHy fluorescence measuring the distance from baseline at 122 s post-stimulation. (*B*) Scatter plots indicate mean ± SEM. ns, not significant, **p* < 0.05 by two-way ANOVA followed by Tukey's multiple comparison test. WT *n* = 15, WT+CDKL5 *n* = 14, KO *n* = 16, KO+CDKL5 *n* = 15 coverslips from 4 independent preparations of neuronal cultures. (*D*) Scatter plots indicate mean ± SEM. ns, not significant, **p* < 0.05 by two-way ANOVA followed by Tukey's multiple comparison test. WT *n* = 20, WT+CDKL5 *n* = 18, KO *n* = 21, KO+CDKL5 *n* = 19 coverslips from 5 independent preparations of neuronal cultures.

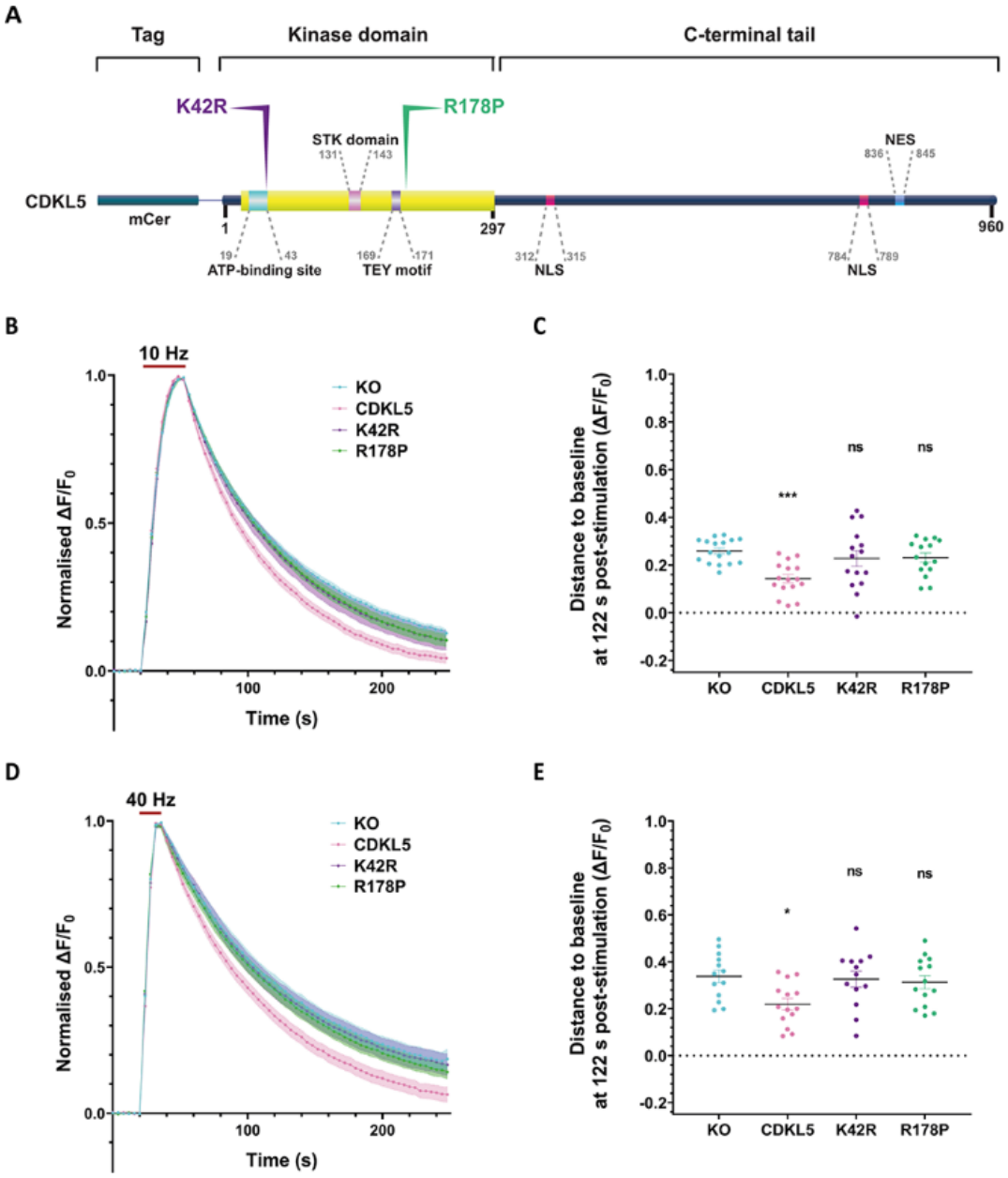

Figure 6. Point mutations within the CDKL5 kinase domain cannot correct SV endocytosis kinetics in CDKL5 KO neurons. (*A*) Schematic representation of the structural domains of CDKL5. Point mutations were introduced into the kinase domain including K42R, within the ATP-binding region, and R178P adjacent to the TEY motif. All constructs were tagged with mCer at their N-termini. (*B-E*) Primary hippocampal neurons from CDKL5 KO rats were co-transfected with sypHy and mCer (KO, light turquoise), mCer-CDKL5 (CDKL5, light pink), K42R (purple) or R178P (green) at 8-9 DIV and used at 13-14 DIV. (*B*,*D*) sypHy response from neurons stimulated (red bar) with either 300 APs at 10 Hz (*B*) or 400 APs at 40 Hz (*D*)

normalised to the stimulation peak. (*C*,*E*) SypHy fluorescence measuring the distance from baseline at 122 s post-stimulation. (*C*) Scatter plots indicate mean ± SEM. ns, not significant, ***$p < 0.001$ by one-way ANOVA followed by Dunnett's multiple comparison test. KO $n = 17$, CDKL5 $n = 16$, K42R $n = 15$, R178P $n = 15$ coverslips from 5 independent preparations of neuronal cultures. (*E*) Scatter plots indicate mean ± SEM. ns, not significant, *$p < 0.05$ by one-way ANOVA followed by Dunnett's multiple comparison test. KO $n = 13$, CDKL5 $n = 14$, K42R $n = 13$, R178P $n = 14$ coverslips from 4 independent preparations of neuronal cultures.

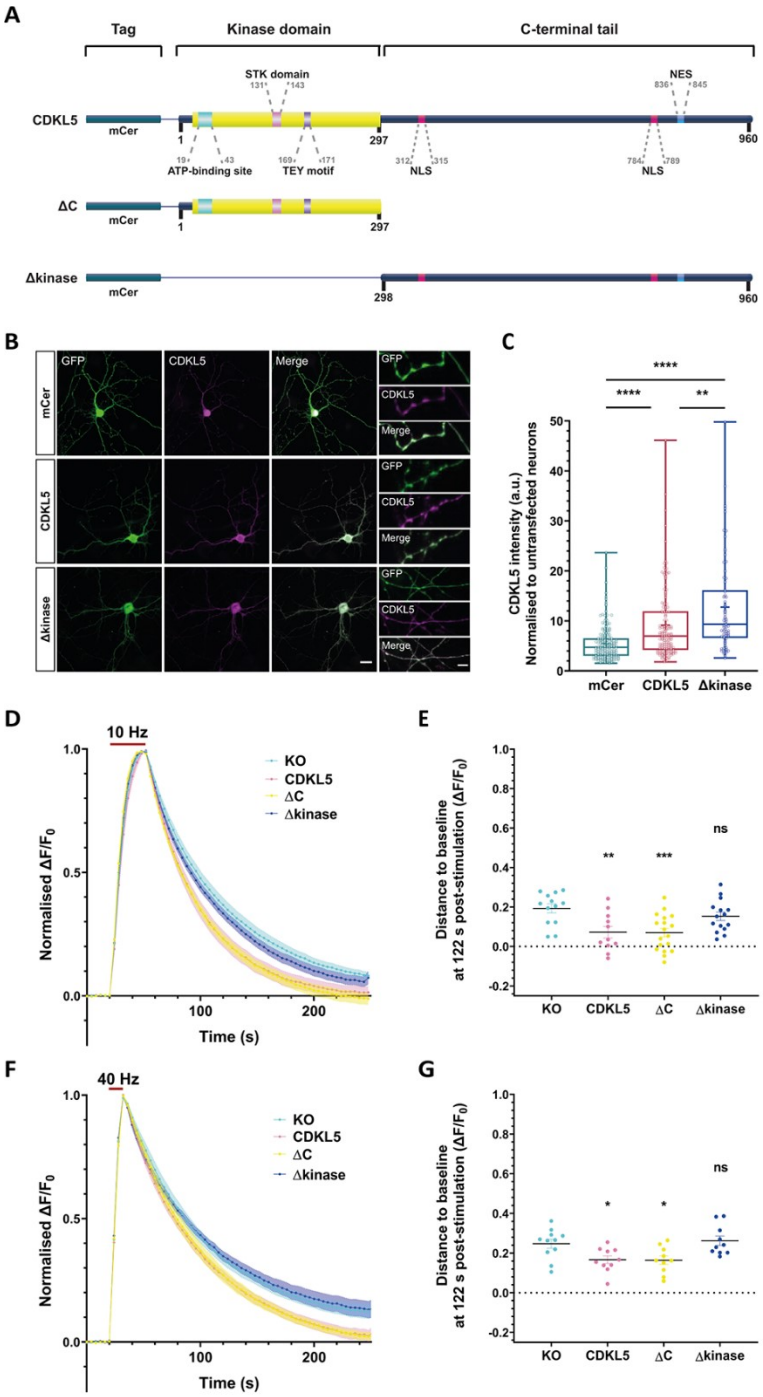

Figure 7. The CDKL5 kinase domain is sufficient to restore the SV endocytosis kinetics in CDKL5 KO neurons. (*A*) Schematic representation of the structural domains of CDKL5. Truncated versions of CDKL5 were generated comprising either the kinase domain (ΔC) or the C-terminal tail (Δkinase). All constructs were tagged with mCer at their N-termini. (*B*) mCer-tagged CDKL5 constructs are expressed in primary hippocampal neurons. Neurons from WT rats were transfected with mCer, mCer-tagged full-length CDKL5, or mCer-tagged Δkinase at 8-10 DIV and were fixed at 15 DIV. Representative images of neurons and axons expressing mCer (control) and either CDKL5 construct labelled for GFP (green) and CDKL5 (magenta). Merged images of GFP and CDKL5. Scale bar, 20 µm (neurons) and 5 µm (axons). (*C*) Quantification of CDKL5 fluorescence intensity of mCer-expressing cell bodies normalised to the intensity of untransfected cell bodies. Box plots present median with IQR

indicating min to max whiskers. ns, not significant, **p < 0.01, ****p < 0.0001 by Kruskal-Wallis test followed by Dunn's multiple comparison test, + indicates mean value. mCer n = 191, CDKL5 n = 149, Δkinase n = 71 cell bodies from 4 independent preparations of neuronal cultures. (D-G) Primary hippocampal neurons from CDKL5 KO rats were co-transfected with sypHy and mCer (KO, light turquoise), mCer-CDKL5 (CDKL5, light pink), the kinase domain (ΔC, yellow) or the C-terminal tail (Δkinase, blue) at 8-9 DIV and used at 13-14 DIV. (*B*,*D*) sypHy response from neurons challenged (red bar) with either 300 APs at 10 Hz (*B*) or 400 APs at 40 Hz (*D*) normalised to the stimulation peak. (*C,E*) sypHy fluorescence measuring the distance from baseline at 122 s post-stimulation. (*C*) Scatter plots indicate mean ± SEM. ns, not significant, **p < 0.01, ***p < 0.001 by one-way ANOVA followed by Dunnett's multiple comparison test. KO n = 13, CDKL5 n = 11, ΔC n = 18, Δkinase n = 15 coverslips from 4 independent preparations of neuronal cultures. (*E*) Scatter plots indicate mean ± SEM. ns, not significant *p < 0.05 by one-way ANOVA followed by Dunnett's multiple comparison test. KO n = 11, CDKL5 n = 10, ΔC n = 10, Δkinase n = 10 coverslips from 3 independent preparations of neuronal cultures.

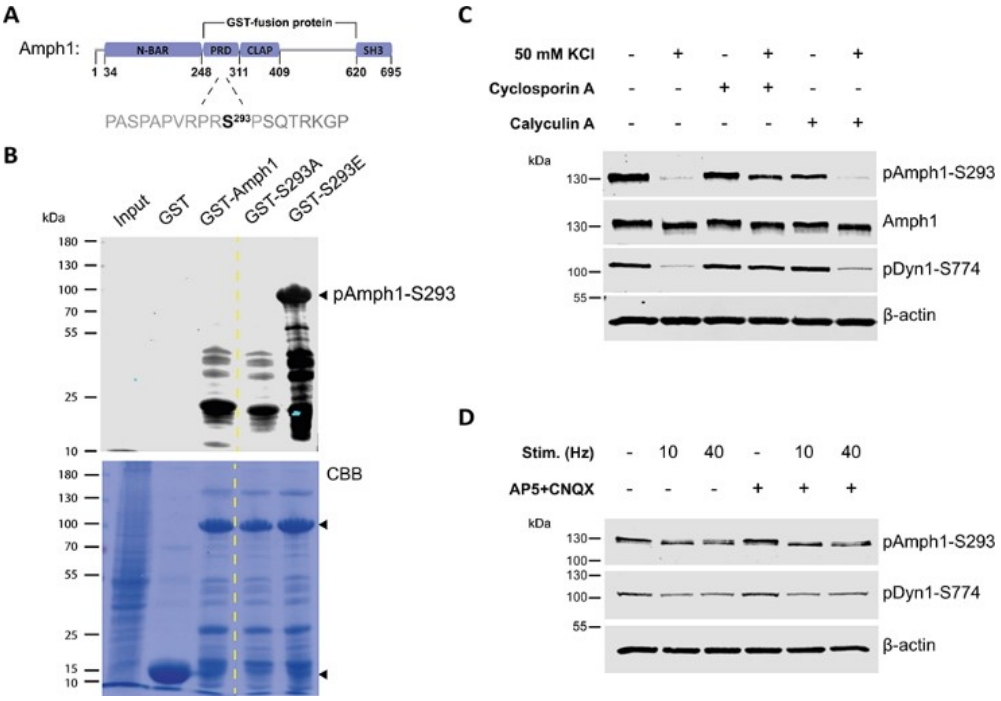

Figure 8. Characterisation of a phospho-antibody to report Amph1-S293 phosphorylation dynamics. (*A*) Schematic representation of the structural domains of human Amph1. The residue S293 is located within the PRD of Amph1. (*B*) The GST-fused phosphomutants of Amph1, S293A and S293E, lacking the N-BAR and SH3 domains, as shown in *A*, were generated and expressed in *Escherichia coli*. The pAmph1-S293 antibody detects robustly only the phosphomimetic S293E fusion protein in synaptosomal lysates. All GST-fused proteins were adequately expressed, as the CBB staining indicates (top arrow). Dashed lines indicate cropped images. (*C*) Hippocampal neurons at 14-15 DIV were stimulated with 50 mM KCl for 2 min to trigger neuronal depolarisation resulting in dephosphorylation of Amph1-S293. Treatment with 10 µM cyclosporin A blocks Amph1-S293 dephosphorylation, but treatment with 100 nM calyculin A fails to prevent dephosphorylation at Amph1-S293. The phosphorylation status at Dyn1-S774 was also tested as this site undergoes activity- and calcineurin-dependent dephosphorylation. (*D*) Hippocampal neurons at 14-15 DIV were stimulated with either 300 APs at 10 Hz or 400 APs at 40 Hz in the presence or absence of 50

µM AP5 and 10 µM CNQX. Dephosphorylation at Amph1-S293 occurs at both stimulation frequencies independently of any postsynaptic activity similarly to Dyn1-S774.

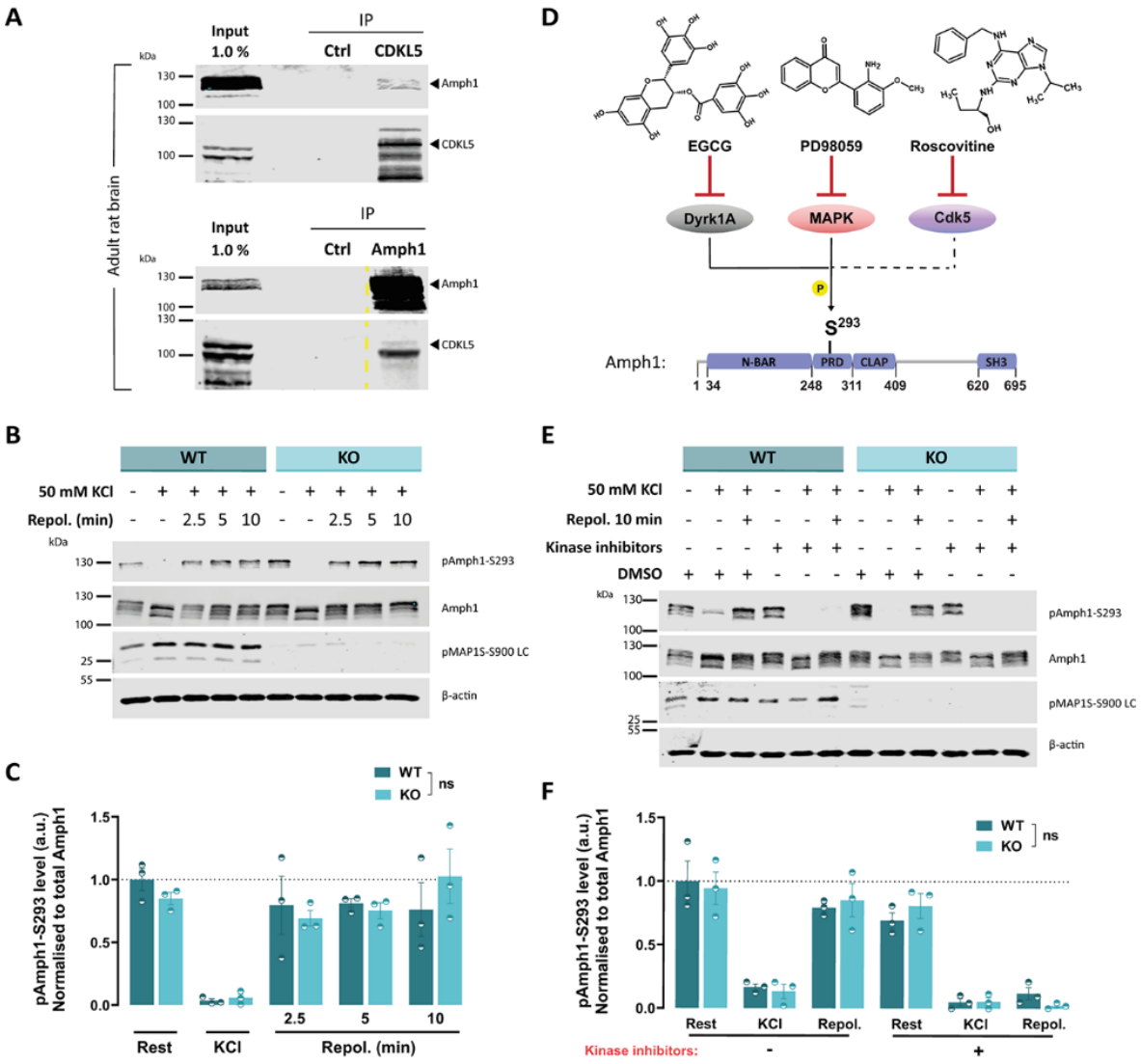

1153 **Figure 9. Amph1-S293 is phosphorylated independently of CDKL5.** (*A*) Co-
1154 immunoprecipitation from adult rat brain lysates of Amph1 and CDKL5 with CDKL5 and
1155 Amph1 antibodies, respectively. Dashed lines indicate cropped images. (*B*) Primary
1156 hippocampal neurons at 14-15 DIV from WT and CDKL5 KO rats were depolarised with 50 mM
1157 KCl for 2 min and allowed to repolarise for 2.5, 5, and 10 min, respectively. Neurons were
1158 analysed for pAmph1-S293, Amph1, pMAP1S-S900 LC, and β-actin. (*C*) Quantification of the
1159 phosphorylation levels of Amph1-S293 normalised to total Amph1. Bars indicate mean ± SEM.
1160 ns, not significant by two-way ANOVA followed by Sidak's multiple comparison test. WT *n* = 3
1161 coverslips/condition, KO *n* = 3 coverslips/condition from 3 independent preparations of

neuronal cultures. (*D*) EGCG, PD98059, and roscovitine were combined to block the kinase activity of Dyrk1A, MAPK, and Cdk5, respectively. All three kinases phosphorylate Amph1 in neurons with Dyrk1A and MAPK (continuous lines) and possibly Cdk5 (dashed line) also targeting S293. The skeletal structures of the inhibitors were generated by ACD/ChemSketch, 2021.1.0. (*E*) Hippocampal neurons at 14-15 DIV derived from WT and CDKL5 KO rats were treated with 20 mM EGCG, 100 µM PD98059, and 50 µM roscovitine inhibitors combined together for 1 h and stimulated with 50 mM KCl prior to repolarisation for 10 min in the presence of kinase inhibitors, or appropriate amount of DMSO. Lysates were assessed for pAmph1-S293, Amph1, pMAP1S-S900 LC, and β-actin. (*F*) Quantification of pAmph1-S293 levels normalised to total Amph1. Background was subtracted in all cases. Bars indicate mean ± SEM. ns, not significant by two-way ANOVA followed by Sidak's multiple comparison test. WT $n = 3$ coverslips/condition, KO $n = 3$ coverslips/condition from 3 independent preparations of neuronal cultures.